

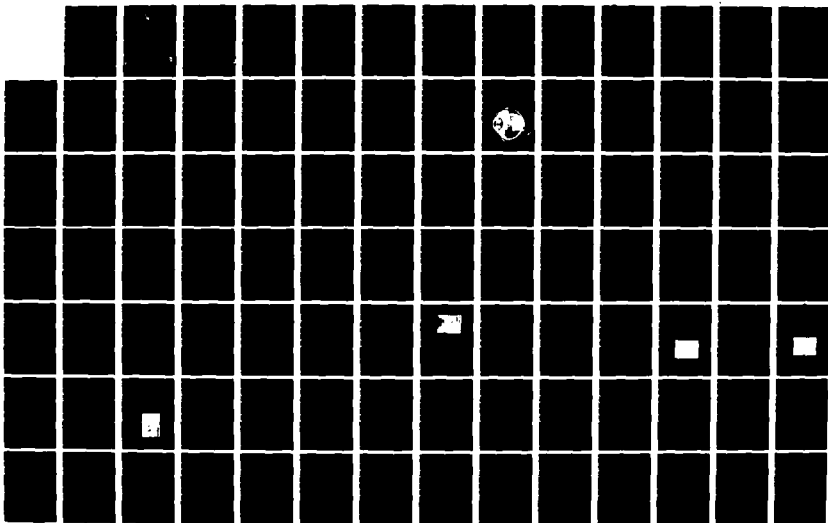
AD-A124 731

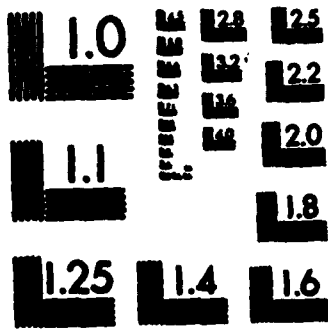
NEODYMIUM: YAG LASER INDUCED SHOCK WAVE OVERPRESSURES
AT THE RETINA(U) AIR FORCE INST OF TECH
WRIGHT-PATTERSON AFB OH SCHOOL OF ENGINEERING
J F TURNER DEC 82 AFIT/GEP/PH/82D-23

UNCLASSIFIED

F/G 6/18

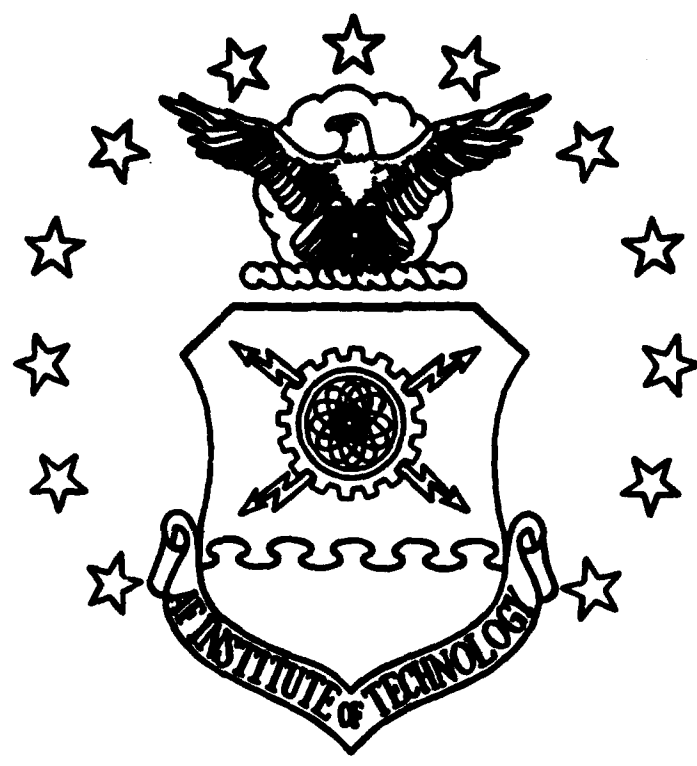
NL





MICROCOPY RESOLUTION TEST CHART
NATIONAL BUREAU OF STANDARDS-1963-A

①



AD A 124 731



DTIC FILE COPY

S DTIC
 ELECTE
 FEB 22 1983 **D**
 E

DEPARTMENT OF THE AIR FORCE
 AIR UNIVERSITY (ATC)
AIR FORCE INSTITUTE OF TECHNOLOGY

Wright-Patterson Air Force Base, Ohio

This document has been approved
 for public release and sale its
 distribution is unlimited.

88 02 022 082

AFIT/GEP/PH/82D-23

NEODYMIUM:YAG LASER INDUCED
SHOCK WAVE OVERPRESSURES
AT THE RETINA
THESIS

AFIT/GEP/PH/82D-23

JOHN F. TURNER
2LT USAF

DTIC
SELECTE
FEB 2 1983
S E D

Approved for public release; distribution unlimited

AFIT/GEP/PH/82D-23

**NEODYMIUM:YAG LASER INDUCED SHOCK WAVE
OVERPRESSURES AT THE RETINA**

**Presented to the Faculty of the School of Engineering
of the Air Force Institute of Technology
Air University (ATC)
in Partial Fulfillment of the
Requirements for the Degree of
Master of Science**

By

**John P. Turner, B.S.
2LT USAF
Graduate Engineering Physics**

December 1982

Accession For	
DTIC SPAN	<input checked="" type="checkbox"/>
DTIC TAB	<input type="checkbox"/>
Unannounced	<input type="checkbox"/>
Justification	
By _____	
Distribution/	
Availability Codes	
Dist	Avail and/or Special
A	



Approved for Public Release; Distribution Unlimited

Preface

This thesis describes an investigation into one aspect of a new application of lasers in the field of ocular medicine--the use of a Nd:YAG laser to remove opacified posterior capsules from lens-implant patients. With this tool, the ophthalmologist has the capability of treating thousands of people in the office rather than in the operating room. The benefits of this type of procedure, and a keen interest in the field of medicine were the prime motivating factors in my decision to explore this area.

This thesis could not have been completed without the help and support of many people, both physically and mentally.

Without a doubt, a special note of thanks must be extended to Dr. Leno S. Pedrotti, my thesis advisor, for his guidance, extreme personal interest, and overall supporting attitude. His input was made all the more special as I was the last in a long line of his thesis students. Also, I wish to thank Lt. Col. William F. Bailey, who assumed the duties of thesis advisor upon the retirement of Dr. Pedrotti, and who also steered my efforts in the right direction on more than one occasion.

I also wish to thank Maj. Michael R. Stamm for his thoughtful questions, and a great deal of assistance. Without him, the EYESHOC code could never have been written.

A very important part of the work done in this project was the actual measurement of the overpressures in a test

cell. This could never have been accomplished without the technical expertise of Ron Gabriel and George Gergal, both of whom I am deeply indebted to.

Thanks must also go to Dr. Richard Keates, Jill McCune, and the rest of the staff at the Ohio State University Eye Clinic; without their hospitality and help, much of this work could never have been attempted.

Finally, I wish to thank Diane for being so supportive, keeping me going when it seemed impossible, and for just being there when I truly needed her the most.

John F. Turner

(This thesis was typed by Ms. Barbara A. Graham.)

Table of Contents

	<u>Page</u>
Preface.....	ii
List of Figures.....	vi
List of Tables.....	vii
List of Symbols.....	viii
Abstract.....	ix
I. Introduction.....	1
Objective and Scope.....	1
Background.....	2
Development.....	6
II. The Eye and Laser Radiation.....	7
Introduction.....	7
Anatomy and Physiology of the Human Eye.....	7
Laser Effects on Ocular Tissue.....	12
Radiative Effects.....	13
Mechanical Effects.....	15
III. The Physics of Shock Waves.....	17
Introduction.....	17
Shock Waves.....	17
Shock Wave Generation.....	19
Shock Wave Propagation.....	21
Shock Wave Effects on Ocular Tissue.....	25
Retinal Effects.....	26
IV. Theoretical Modeling of a Shock Wave in the Eye.	30
Introduction.....	30
One-Dimensional Hydrodynamics Code.....	31
Governing Equations.....	31
Assumptions.....	32
Lagrangian Mesh.....	34
Computer Model of the Human Eye.....	37
Assumptions.....	37
Code Discussion.....	39
Initial Conditions.....	41
Code Validation.....	43
Predicted Results.....	44
V. Experimentation.....	47

	<u>Page</u>
System Design.....	47
Laser System.....	47
Pressure Transducer and Associated Electronics.....	51
Test Cell and Vitreous Model.....	54
Experimental Procedures.....	58
 VI. Results and Discussion.....	 61
Overpressures versus Energy.....	61
Overpressures versus Distance.....	62
Comparison of Predicted versus Measured Overpressures.....	65
 VII. Recommendations and Conclusions.....	 71
Shock Code Limitations and Proposed Changes....	72
Future Experimentation.....	73
Clinical Conclusions.....	75
 Bibliography.....	 77
 APPENDIX A: Calculation of γ for Water.....	 80
 APPENDIX B: Elimination of Specific Internal Energy in Time Derivative of Pressure.....	 82
 APPENDIX C: Calculation of Time Step Based on Local Adiabatic Speed of Sound.....	 84
 APPENDIX D: Calculation of First Cell Specific Internal Energy and Pressure.....	 86
 APPENDIX E: EYESHOC Code Listing and Sample Output...	88
 APPENDIX F: Modeling a Point Explosion Using EYESHOC.	93
 Vita.....	 97

List of Figures

<u>Figure</u>		<u>Page</u>
1	The Human Eye.....	8
2	Photopic and Scotopic Luminous Efficiency Curves for the Eye.....	11
3	Initial State, Density and Velocity Profiles of a Shock Wave.....	19
4	The Piston Driven Shock Front.....	22
5	The Shock Discontinuity.....	24
6	Lagrangian Mesh Development Scheme.....	35
7	Lagrangian Cells and Cell Variables Used in EYESHOC.....	36
8	Pressure versus Distance Plots for Various Times.....	42
9	Pressure Drop Across Front versus Shock Wave Radius.....	45
10	Test System Schematic.....	48
11	Test System Photograph.....	49
12	Laser Oscillator Schematic.....	52
13	Pressure Transducer.....	53
14	Test Cell.....	55
15	Cell Front Transmission Data.....	57
16	Test Cell with Attached Pressure Transducer...	58
17	Overpressure versus Energy.....	64
18	Overpressure Times Distance Squared versus Distance.....	67
19	Comparison of Predicted and Measured Over-Pressures.....	69
E-1	Sample Output from EYESHOC.....	92
F-1	Comparison of Pressure Drop Across Front versus Shock Wave Radius for EYESHOC and Sedov.....	95

Figure

Page

F-2 Comparison of Density Behind Wave Front
 versus Shock Wave Radius for EYESHOC
 and Sedov..... 96

List of Tables

<u>Table</u>		<u>Page</u>
I	EYESHOC First Cell Specific Internal Energy and Pressure Values for Test Runs.....	43
II	Predicted Overpressures at the Retina for EYESHOC Test Runs.....	46
III	Overpressures versus Energy Deposited at Focal Point for Varying Distances from Retina.....	63
IV	Overpressures Times Distance Squared for Varying Energy Levels at Focal Point.....	66
V	Comparison of EYESHOC Predictions and Measured Overpressures.....	68

List of Symbols

a	Constant Spreading Shock Wave Over Several Cells
BSS	Balanced Salt Solution
C	Spec. of Sound in the Unshocked Material
C_p	Specific Heat at Constant Pressure
C_v	Specific Heat at Constant Volume
D	Gas Velocity Immediately in Front of a Piston
E	Specific Internal Energy of a Material
k	Boltzmann's Constant
m	Molecular Weight of a Material
p	Pressure of a Material
p₀	Ambient Pressure of an Unshocked Material
q	Artificial Viscosity
r	Radius of a Spherical Shock Wave
S	$\dot{\gamma}$
T	Absolute Temperature
t	Time
u	Piston Velocity
V	Specific Volume -- Reciprocal of Density
V₀	Initial Specific Volume -- Reciprocal of Initial Density
α	Volume Coefficient of Expansion
γ	Ratio of C _p to C _v
$\gamma - 1$	$\gamma - 1$
K	Isothermal Compressibility
ρ	Density of the Material
ρ_0	Density of the Unshocked Material

Abstract

The use of a neodymium:YAG laser to open opacified posterior capsules in the human eye was examined. In particular, this study involved the development of a one-dimensional hydrodynamic code to model the propagation of the shock wave in the vitreous, and the measurement of overpressures induced in a model system.

The model system consisted of balanced salt solution in a cubical test cell. A pressure transducer was affixed to the rear of the cell, and 15 nsec Q-switched laser pulses were focused at distances of 6, 8, 10, and 14 mm from the transducer to initiate shock waves. Overpressures were measured for pulse energies of 3.75, 7.50, and 22.50 mJ at the focal point. The balanced salt solution was chosen because it resembles the vitreous in breakdown characteristics, and the 14 mm distance is significant since it approximates the distance from the posterior capsule to the retina.

Overpressures ranging from 0.018 - 0.432 atm were recorded at the transducer. The code was tested for a pulse energy of 3.75 mJ and predicted a pressure change of 2%, in excellent agreement with measured values. For pulse energies of 7.50 and 22.50 mJ, the maximum deviation was 5% from measured pressure differences.

Based on current research by ophthalmologists using such laser systems for treatment, it is concluded that overpressures of 0.10 atm or less cause no retinal damage.

c

I. Introduction

Recent advances in the integration of lasers into the field of ophthalmology have aided in the facilitation of patient care. One of these, the use of a neodymium YAG (Nd:YAG) laser to remove opacities in the posterior capsule, has helped to move many patients from the operating room to outpatient care facilities. This thesis examines, in detail, one consequence of using a Nd:YAG laser to perform such an operation.

Objective and Scope

This paper will analyze the shock wave generated in the eye when high peak power, nanosecond laser pulses are focused in the posterior chamber of the human eye. The formation and propagation of shock waves in the posterior chamber of the eye are modeled and effects on ocular tissue are evaluated. The theoretical portion of this thesis will develop a one-dimensional hydrodynamic code in spherical coordinates using a lagrangian mesh to model the propagation of a shock wave through the eye from the posterior capsule to the retina. The experimental portion of the thesis will involve attaching a pressure transducer to a test cell filled with balanced salt solution to measure the pressure variations induced by the pulses of a Q-switched Nd:YAG laser.

The purpose of this investigation is two-fold. First, because the surgical procedure is currently being performed

with Nd:YAG lasers, an analysis of the possible damage levels at the retina due to the presence of the shock wave is mandatory. Second, a correlation between pulse energies focused in the posterior chamber and actual pressure increases at the retina is highly desirable. This thesis will develop a maximum level of acceptable overpressure at the retina during Nd:YAG laser-assisted posterior capsulotomies. This maximum level will be based on predicted results, measured values, and current research by practicing ophthalmologists.

Background

The procedure being investigated has developed from studies on the alleviation of post cataract surgery complications. In such cataract operations, a surgeon often removes the occluded lens from the patient's eye, and the lens is replaced by external spectacles or contact lenses. However, increasing numbers of ophthalmologists are now using intraocular lens (IOL) implants, after cataract removal, in place of or in addition to, spectacles or contact lenses. There are currently two methods of lens implantation in use, the posterior chamber method, and the anterior chamber method. The posterior chamber method, the most common of the two methods, involves placing the IOL in the area vacated by the patient's own lens (Ref 1:271). The anterior chamber method of implantation places the IOL anterior to the original lens cavity, and requires either clipping the IOL to the iris (iris clip IOL), or allowing

extensions into the posterior chamber to hold the implant in position (iridocapsular IOL) (Ref 2:58).

For many lens implant recipients, a serious complication may arise. The posterior capsule, immediately behind the patient's lens, opacifies, and reduces the patient's vision greatly, for both types of IOL implants. Until recently, only further surgery could remove the opacified capsule and restore some degree of normal vision to the patient. However, in the past two years, work began on the use of a laser to open the capsule. By using a laser, no surgery in which the patient requires hospitalization is necessary, the extent of patient discomfort is minimal, and the laser-assisted procedure is accomplished virtually within minutes.

In 1980, Aron-Rosa of France began a study using a laser system to open the posterior capsule of lens implant patients (Ref 3). This system is a mode-locked Nd:YAG laser which emits 30 picosecond pulses enclosed in an envelope whose pulsewidth is 20 nanoseconds, and is operated at a one Hertz rep rate. The laser is focused to a spot of 50 microns in diameter, and yields energies per pulse of 3 to 4.5 millijoules. These values convert to power densities of 1×10^{17} to 1.6×10^{17} W/cm² at the focus.

The results obtained by Aron-Rosa were very significant. Twenty post lens-implant patients were subjected to the laser procedure for opening the posterior capsule. A series of five to ten laser pulses were focused on the capsule, and no deleterious effects were noted, including no IOL implants

being shattered. Effects such as small markings and scratches were seen on the implants, however these would in no way interfere with a patient's vision. Specifically, no permanent intraocular pressure rise was noted due to the laser induced shock wave, and no lesions were induced on either the cornea, iris, vitreous, or retina. Most importantly, visual improvement was achieved in each patient, with visual improvement as great as 4/200 to 20/20 being noted.

In 1981, Fankhauser, van der Zypen, and associates used a similar system in Germany to investigate ocular treatments closely related to the opening of the posterior capsule. The operations described by Fankhauser, et. al., included opening pupillary membranes and operations on the iris (Ref 4).

In early 1982, Lt. James Riggins of the Air Force Institute of Technology, conducted a feasibility study under the direction of Dr. Richard Keates of the Ohio State University Eye Clinic and Dr. Leno S. Pedrotti of the Air Force Institute of Technology, investigating the use of a Q-switched laser system to open opacified posterior capsules (Ref 5). In addition, the study investigated the use of the same laser system to break vitreous strands, or cellular striations present in the vitreous humor.

This system delivered a maximum pulse energy of 10.89 millijoules in a pulsewidth of 27 nanoseconds focused in a spot of diameter 4.4 microns to yield a peak focused power density of 2.65×10^{12} W/cm². Experimental results indicated

that the system could open opacified capsules, and also that glass IOL implants would be shattered if the IOL were in direct contact with the capsule during the procedure. Theoretical calculations also led to the conclusion that vitreous strands located no further than 4-6 mm from the posterior capsule could be ruptured in an undilated eye -- an eye whose pupil is the smallest, and therefore represents the worst case--without possible damage to the retina from laser energy deposition.

The work previously accomplished clearly indicates that a Nd:YAG laser can be used to open an opacified posterior capsule in a lens implant patient. The mechanism is the creation of a spark plasma and an associated shock wave. It is the characterization of this shock wave which is needed at this juncture in the research. According to Dr. Sidney Lerman, Professor of Ophthalmology, Emory University,

"I would strongly recommend such an approach; i.e. pressure measurements followed by spectroscopic and histopathologic evaluation particularly of the vitreous with respect to the former and the retina with respect to the latter in order to come to some reasonable conclusion regarding the safety of this form of therapy for general clinical use." (Ref 6:6)

This thesis is directed toward a better understanding

of the generation and propagation of the shock wave, and its effect on critical parts of the eye, especially the retina.

Development

This thesis will integrate a portion of the study of hydrodynamics with the basic anatomy and physiology of the human eye. Chapter II will present the physiology of the eye and the effects of a laser on ocular tissue. Chapter III will deal with shock waves, discussing their generation and propagation, and possible effects in the eye.

Chapter IV will begin the major thrust of the thesis, with a discussion of the hydrodynamic code written to model shock propagation in the eye. Chapter V will explain the actual experimental systems and procedures used to measure pressure levels after shock generation, and Chapter VI will present the measured results and evaluate their validity based upon predicted data. Finally Chapter VII will give clinical conclusions and recommendations for additional research and follow-up studies.

II. The Eye and Laser Radiation

Introduction

The human eye is a very complex optical system designed to provide visual sensory input to the brain. It is perhaps the most important organ dedicated to the senses, and any discussion of the eye, or processes occurring therein, must begin with a detailed examination of the eye itself. This chapter begins with a discussion of the anatomy and physiology of the eye, then presents the effects of laser radiation on ocular tissue, from both mechanical and radiative viewpoints. With a firm understanding of the underlying physiology of the eye, a discussion of the physics affecting the organ can then proceed.

Anatomy and Physiology of the Human Eye

From an optical standpoint, the human eye is essentially a positive lens system which collects light rays and focuses them to form a real image on a light sensitive surface (Ref 7:138-141). Figure 1 shows the basic anatomical arrangement of the eye. The eye is almost spherical, and is housed in a tough shell called the sclera. The sclera is white and opaque to light except for the front portion, the cornea, which is transparent. It is the cornea which serves as the first element of the lens system. The curvature of the cornea serves to direct light entering the eye through the anterior chamber which contains a clear

watery fluid called the aqueous humor. Contained within the aqueous is the portion of the eye -- the iris -- which gives the eye its color. The iris is a diaphragm which controls the amount of light entering the eye by expansion or contraction of the pupil. The iris can close the pupil in bright light to approximately 2 mm in diameter, or expand it in darkness to about 8 mm in diameter. Also, the iris contracts to increase image sharpness when the eye is used for close work.

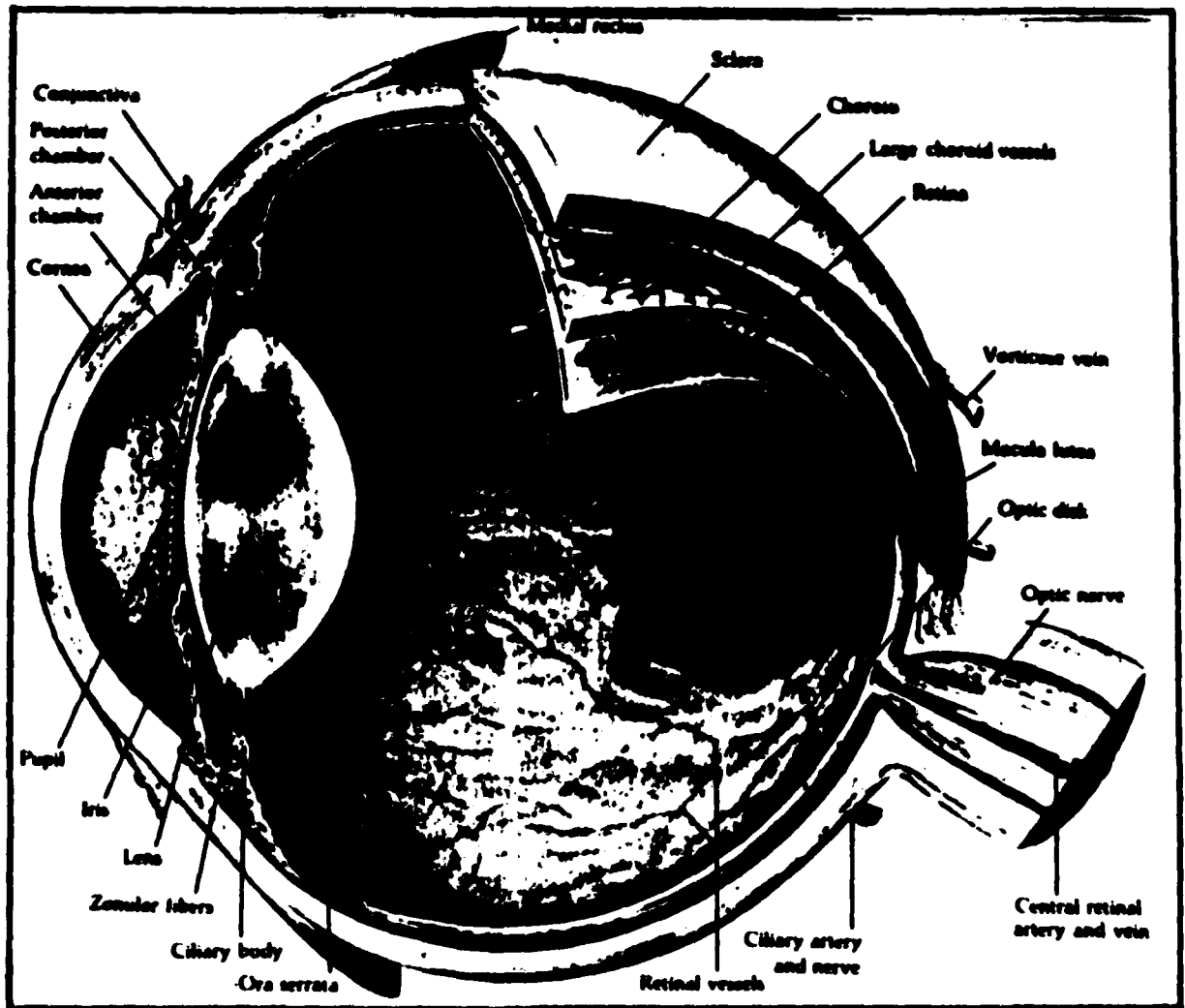


Figure 1. The Human Eye (Ref 8:32)

Immediately behind the iris is the crystalline lens. The lens is enclosed in an envelope -- the so-called lens capsule -- which has walls approximately 10 microns thick. The capsule segment facing the iris is the anterior capsule, while the segment to the rear of the lens is the posterior capsule. The lens itself has the size and shape of a small bean, and is formed of approximately 22,000 layers. The lens is initially very pliable; however this pliability decreases as the eye ages. Posterior to the lens and its capsule is another chamber filled with a transparent substance composed mostly of water, the vitreous humor. The vitreous provides support for the retina while allowing light and nutrients to diffuse from the anterior portion of the eye to the posterior portion (Ref 9:252).

Within the sclera is an inner layer called the choroid. This is a dark shell containing blood vessels and melanin, a dark brown or black pigment. It is this pigment which gives the choroid its property of acting as an absorber of stray light rays in the eye. Near the back of the eye, a layer of light receptor cells covers much of the inner surface of the choroid to a depth of approximately 0.51 mm. This layer is known as the retina. A focused beam of light is absorbed in this structure through electrochemical reactions occurring in the two types of photoreceptor cells present, rods and cones. Approximately 125 million of these cells are contained heterogeneously in the retina. The rod cells are highly sensitive and can respond to very dim

light, however these cells do not distinguish colors and relay only ill-defined images. The cone cells, of which there are 6-7 million, give detailed color images in bright light, but do not respond to images at lower light levels.

Contained within the retina is the point of exit of the optic nerve from the eye. This region contains no receptor cells and therefore does not contribute to the visual process. This area is called the blind spot for this reason. The optic nerve enters the eye at the blind spot and spreads out over the back of the interior of the eye. This extension of the optic nerve is the retina itself.

Just as there is a portion of the retina which offers no receptor cells, so there is a portion in which the cones are thinner and more densely packed than anywhere else. This is a tiny rod-free region approximately 0.3 mm in diameter in its center known as the fovea centralis. The fovea lies at the center of the yellow spot or macula, a small depression 2.5-3 mm in diameter at the center of the retina. The make-up of the fovea allows it to provide the sharpest and most detailed visual information. This causes the eye to move continuously so that the light coming from the object to be seen is directed onto the fovea. However, the image directed onto the fovea is not kept stationary on one set of photoreceptors, but rather is constantly shifted across different cells. If the image were stationary, it would eventually fade out as the nerve cells to which the photoreceptors are attached reached saturation -- due to

over-stimulation -- and ceased to respond. This is mainly due to the fact that the cones in the fovea are individually connected to nerve fibers, while in contrast, rods are multiply connected to nerve fibers, and any one fiber can be stimulated by any one of approximately one hundred rod cells. The shifting of images across the fovea results in the fact that the visualization of any object is a construction of the ocular system based on a continuous analysis of a time-varying retinal image.

Figure 2 shows the luminous efficiency of the eye. Both photopic (adapted for vision in bright light), V , and scotopic (adapted for vision in dark light), V' , luminous

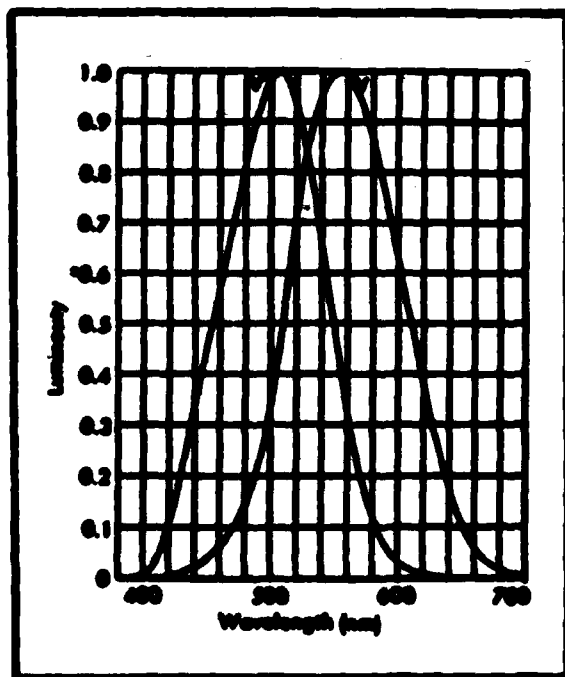


Figure 2. Photopic and Scotopic Luminous Efficiency Curves for the Human Eye (Ref 9:362)

efficiency curves are shown. The most efficient wavelength in a light-adapted eye is 555 nm, while in a dark adapted eye it is 510 nm. The efficiency of all other wavelengths is given as a decimal fraction of the most efficient wavelength (Ref 9:352). The normal wavelength range of human vision is approximately from 390 nm to 780 nm. However, these limits have been extended to about 310 nm in the ultraviolet and 1050 nm in the infrared by some studies (Ref 5:140). The ultraviolet transmission limit is determined by the lens, which absorbs in the UV. Patients such as those with whom this thesis is concerned -- who have undergone surgical lens removal -- experience greatly improved UV sensitivity.

Laser Effects on Ocular Tissue

Two main areas of specific effects result when the energy from a laser is deposited in the eye. These effects can be classified as radiative and mechanical effects. Radiative effects essentially involve thermal and/or photochemical changes following energy deposition while mechanical effects deal with damage resulting from acoustical waves or hydrodynamic shock waves. Even though only mechanical effects are involved in the disruption of opacified posterior capsules, both types of effects will be examined in this chapter.

Radiative Effects

As stated, radiative effects involve both thermal and photochemical damage mechanisms. The most thoroughly studied, and adequately modeled, of these two damage mechanisms is that associated with thermal effects. This type of injury accompanies energy absorption in the retina and choroid after focusing by the lens system of the eye (Ref 8:81). The heat generated as a result of energy absorption has two means of leaving the focal area - diffusion and conduction by blood flow. If the rate of heat generation exceeds the rate of heat conduction, the temperature of the tissue rises. If the temperature exceeds the biologic tolerance of the tissue, damage manifests itself as burning and/or lesion formation.

This type of control on thermal damage has been studied by van der Zypen, Fankhauser, and associates (Ref 11:59-180). They argue against an increase in temperature above the boiling point in the iris -- under conditions of continuous exposure -- due to the fact that local evaporation initiates fluid circulation in both anterior and posterior chambers, whereby hot fluids leave the absorption region while cold fluids enter. This gives rise to a mechanism which limits the temperature of the absorbing area. If a vapor layer forms between the absorbing particles and the conducting fluids however, the temperature limiting mechanism fails and temperatures above the boiling

point may be reached. Theoretical predictions based on a water model and subsequent experiments conducted using water as the circulating fluid have verified the accuracy of the temperature limiting mechanism (Ref 11:88). The experiments were conducted using a continuous wave (cw) argon laser yielding 0.75 Watts in a focal spot of 30-100 microns in diameter (Ref 11:89-90).

Either general damage mechanism -- radiative or mechanical -- is highly dependent upon the time of exposure. This is due to the fact that for longer exposures, more of the energy is absorbed and interacts with the tissues undergoing irradiation. If exposures of more than a few seconds are being considered, then evidence indicates that a damage mechanism referred to as "photochemical" becomes dominant (Ref 10:84). These effects are primarily associated with blue and ultraviolet light, and involve light whose photon energies correspond to the binding energies of cell constituents resulting in the breaking of molecular bonds or the initiation of chemical reactions in the tissue surrounding the focal spot (Ref 12:1269).

Photochemical damage manifests itself in various ways depending on the ocular tissue involved. The damage mechanism in the retina is the formation of a lesion, while damage in the cornea involves destruction of epithelial cells, or in some more severe cases, corneal opacification (Ref 13:108-110). Photochemical damage to the lens, which may require a great deal of time to appear, depending on

the dose involved, manifests itself as the destruction and degradation of lens materials, leading to permanent opacifications of the lens (Ref 13:106, 112-114). Such lens opacifications are commonly referred to as cataracts.

Mechanical Effects

As exposure times become shorter, mechanical effects may become significant and lead to damage. However, much controversy still surrounds the extent of this type of damage. Two sources of mechanical damage exist, acoustical waves and shock waves. Both are caused by the absorption of a great deal of energy in a very short time period. However the shock wave propagates at a velocity greater than the local speed of sound while the acoustical wave propagates at a velocity equal to the local sound speed (Ref 14:111).

Extensive research by Cleary and associates (Ref 15:175-219) on acoustical wave propagation and damage has indicated that damage due to these transients can be expected over a much larger area than would be noticed from thermal damage alone. Also, it must be noted that while the two types of pressure transients under discussion are normally considered as separate quantities, a shock wave will degenerate into an acoustical wave if the density of the surrounding medium is sufficiently high, or if the time interval of propagation is sufficiently long. Research conducted by van der Zypen, Fankhauser, and associates has indicated that shock wave formation in the iris can create hemorrhaging, cell fragmen-

tation, and the ejection of blood cells into the surrounding tissue (Ref 11:135-136). A similar type of damage is seen on the retina.

The above discussion of the anatomy of the eye and its reactions to laser radiation has laid the necessary groundwork for this study. Now we must examine the physics of shock waves before we can fully understand the processes which occur when a shock wave is created in the vitreous humor or the posterior capsule. Chapter III provides this information.

III. The Physics of Shock Waves

Introduction

At this point, we have gained an understanding of the human eye as an organ dedicated to providing visual sensory input to the brain. However, when the energy from a Nd:YAG laser pulse is deposited in the posterior capsule or adjacent vitreal tissue, the main processes of interest become more physical, and less biological, in nature. This chapter will provide the material necessary to understand the physical nature of a shock wave, both in terms of its generation -- how a shock wave is created -- and its propagation -- how a shock wave moves through the surrounding medium. In addition, the possible effects caused by a shock wave in various parts of the eye will be discussed.

Shock Waves

In the following discussion, the terms fluid and gas will often be used interchangeably to denote the medium in which the shock is propagating. This is often encountered in fluid dynamics, where a fluid is considered any substance which flows, and a gas is a subset of the overall class of fluids.

A discussion of shock waves is best begun by examining a gas initially at rest, with constant density ρ_0 and pressure p_0 , bounded on the left by a plane piston. Assume now that the piston moves to the right with velocity u ,

such that the gas is compressed. Three basic gas dynamic equations govern the motion of the gas either prior to the motion of the piston or after compression begins. These are the equations of continuity, the equation of momentum conservation, and the equation of energy conservation of a small group of fluid particles commonly located near a point x at a time t (Ref 16:104).

$$d\rho/dt = -\rho(\nabla \cdot u) \quad (1)$$

$$du/dt = -\rho^{-1}(\nabla p) \quad (2)$$

$$dE/dt = -\rho^{-1}(\nabla \cdot u) \quad (3)$$

respectively, where,

u = average velocity (cm/sec)

ρ = average mass density (gm/cm³)

p = average pressure (erg/cm³)

E = average specific internal energy (erg/gm)

If an attempt is made to find a continuous solution for the case of a piston with no initial velocity such that the velocity of the piston is discontinuous, no physically realistic solution is available. However, a solution can be found if it is assumed that the variables u , ρ , and p are discontinuous across a boundary which defines regions where the gas is undisturbed -- $u = 0$, $p = p_0$, $\rho = \rho_0$ -- and where the gas immediately adjacent to the piston moves with velocity equal to the piston velocity (Ref 17:45). Such a solution is shown in Figure 3.

In this type of solution to the gas dynamic equations, the transition from undisturbed gas to compressed gas occurs almost instantaneously over such a thin region that the discontinuous model is in many cases quite valid. This type of discontinuity is known as a weak shock. While Equations (1) - (3) for an ideal fluid predict the development of a shock, they become meaningless at a shock and cannot be used for its complete treatment. If the viscosity of the medium is introduced in the equations, the overall discontinuity of the solution relaxes to a point where the equations can be solved to predict shock-transition details (Ref 18:35).

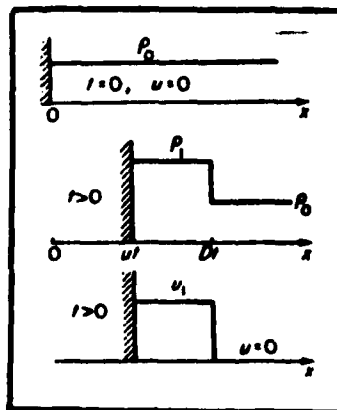


Figure 3. Initial State, Density, and Velocity Profiles of a Shock Wave (Ref 17:45)

Shock Wave Generation

Various phenomena are associated with the generation of a shock wave. The movement of a piston through an undisturbed gas has been mentioned -- and will be examined in

detail subsequently -- but this is not the only means of creating a shock wave. Another method of shock generation involves a strong explosion, in which a great deal of energy is deposited in a small volume in a very short time interval (Ref 15:93-101). It is this type of shock, referred to as a detonation or reactive shock, that is generated when an energy pulse from a Nd:YAG laser is deposited quickly in the posterior capsule of the eye. Several theories have been offered concerning the shock wave accompanying plasma formation. Theorized wave types include a detonation wave driven by plasma absorption and a radiation transport wave in which the radiated thermal energy from the plasma acts to ionize material behind the plasma which then absorbs laser radiation (Ref 19:68, 70). Normally such an absorption wave, also known as a laser supported detonation wave, exists when the laser energy is being provided by a continuous beam rather than a pulsed beam. This is due to the fact that with continuous wave (cw) radiation, the plasma is constantly being fed with energy that must be absorbed, while with a pulsed beam, the energy input is not constant, and the plasma can dissipate if the time between laser pulses is great enough.

The shock waves resulting from laser induced plasma formation have been studied by several research scientists (Ref 20; 21). Velocities ranging from 2×10^5 cm/sec to 1.6×10^6 cm/sec and pressures as high as 250 kbar (1 bar = 0.9869 atm = 9.97×10^5 erg/cm³) have been reported using

both Nd:YAG and ruby lasers whose powers were usually less than 5MW, but occasionally as high as 30 MW (Ref 20:282; 21:46). All of these values were obtained using water as the medium in which the plasma was formed and the associated shock wave was developed.

Shock Wave Propagation

In order to gain an understanding of how a shock wave propagates in a medium, the example of the piston-driven shock will be examined in detail. The piston shock rather than the reactive shock will be examined because the piston shock can be described by Cartesian coordinates while the reactive shock is often described by spherical coordinates. The difference arises in the fact that for spherical shock waves, the pressure front moves outward radially from the plasma, assuming a $1/r^2$ dependence in a homogeneous medium where r is the distance from the plasma center to the leading edge of the shock front. This $1/r^2$ dependence is not present in the piston driven shock, thereby making it a much more easily understood example for illustrative purposes.

Returning to the case of the moving piston, recall that the piston is moving with a velocity u , and is forming a layer of gas ahead of it, as illustrated in Figure 4.

In this example, following the treatment of Stamm, (Ref 16:114-116), after a given time t , a mass of gas per unit area expressed as $\rho_0 Dt$ (gm/cm^2) where D is the velocity of the gas, is piled up in front of the piston. D must

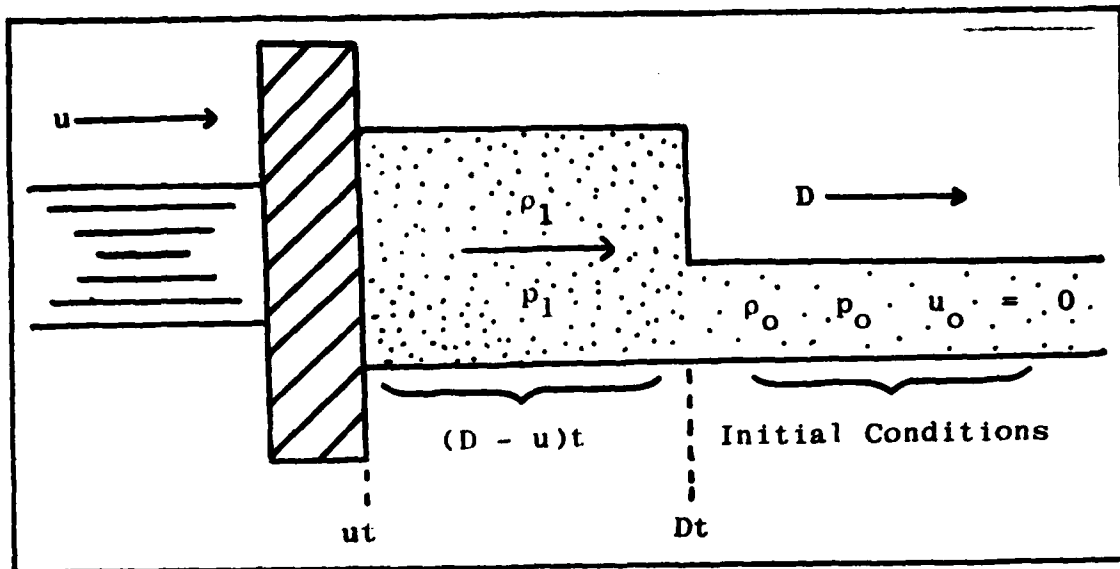


Figure 4. The Piston Driven Shock Front

necessarily be greater than u to account for the accumulation of gas. The gas is compressed into a length given by $(D-u)t$ with a density of ρ_1 . This forms the compression region mentioned previously. The conservation of mass requires that the total uncompressed mass equal the total compressed mass, or,

$$\rho_1(D-u)t = \rho_0 Dt \quad (4)$$

which is another form of the equation of continuity. In a similar manner, we can obtain the equation of momentum conservation by recognizing that the mass will acquire a momentum per unit area given by $\rho_0 Dtu$ (gm/sec-cm) which must equal the impulse per unit area, given by $(p_1 - p_0)t$, so that,

$$\rho_0 Dtu = (p_1 - p_0)t \quad (5)$$

Finally, if the increase in total energy of the compressed gas is considered, this must equal the energy added to the gas by the action of the piston, as dictated by the equation of energy conservation. This means that,

$$p_1 u t = \rho_0 D t (E_1 - E_0 + \frac{1}{2} u^2) \quad (6)$$

where,

$\rho_0 D t$ is the mass per unit area

$E_1 - E_0$ is the internal energy per unit mass (erg/gm)

$\frac{1}{2} u^2$ is the kinetic energy per unit mass (erg/gm)

In order to cast the three equations we have presently into a set that more closely resemble Equations (1) - (3), we must transform the coordinate system of interest from the one illustrated in Figure 4 to one moving with the shock front at a velocity D . This is done by defining new velocity variables u_0 and u_1 such that,

$$u_0 = -D \quad (7)$$

$$u_1 = -(D-u) \quad (8)$$

where,

u_0 = the velocity of the gas flowing into the discontinuity

u_1 = the velocity of the gas flowing out of the discontinuity

This new coordinate system is illustrated in Figure 5.

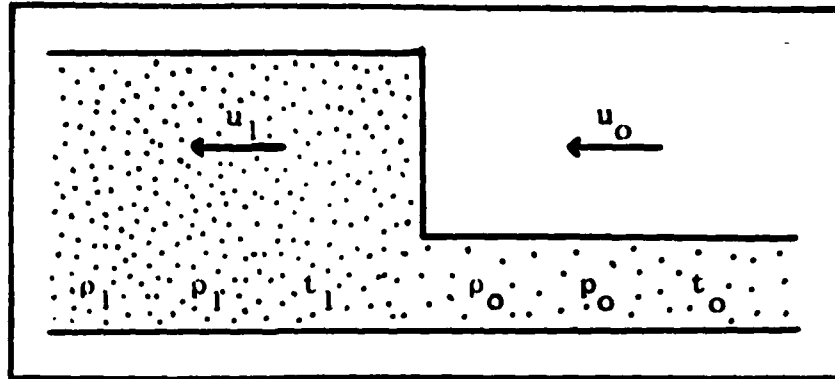


Figure 5. The Shock Discontinuity

In this new coordinate system, the gas dynamic equations -- the equation of continuity, the equation of momentum conservation, and the equation of energy conservation, respectively -- can be expressed as,

$$\rho_1 u_1 = \rho_0 u_0 \quad (9)$$

$$p_1 + \rho_1 u_1^2 = p_0 + \rho_0 u_0^2 \quad (10)$$

$$E_1 + p_1/\rho_1 + \frac{1}{2}u_1^2 = E_0 + p_0/\rho_0 + \frac{1}{2}u_0^2 \quad (11)$$

For any given set of initial conditions, another equation is required to completely describe the motion of the gas. This is required since we have three equations and four unknown quantities -- ρ_1 , u_1 , p_1 , and E_1 . This is the equation of state, which gives a relation between the internal energy E and the pressure p , both for the ambient gas (E_0 , p_0) and for the compressed gas (E_1 , p_1). For an ideal gas, the equation of state is given by,

$$(\gamma-1)E = p/\rho = kT/m \quad (12)$$

where,

k = Boltzmann's constant (1.38×10^{-16} erg/ $^{\circ}$ K)

T = the absolute temperature ($^{\circ}$ K)

m = the molecular weight of the gas (gm)

and,

$$\gamma = C_p/C_v \quad (13)$$

where,

C_p = the specific heat of the gas at constant pressure (erg/gm- $^{\circ}$ K)

C_v = the specific heat of the gas at constant volume (erg/gm- $^{\circ}$ K)

At this point, we could analyze any gas or liquid in which a shock wave is propagating, if we had the true equation of state, which often differs from the ideal gas condition of Equation (12).

Shock Wave Effects on Ocular Tissue

While many investigations have been conducted in an attempt to quantify the amount of damage directly attributable to laser induced shock waves, very little definitive information is available. This seems to follow because in most of the reported experiments, the system under study, e.g. the retina, was of a sufficiently complex nature that it was not possible to differentiate between the effects of other sources of tissue disruption -- thermal denaturation,

vaporization, and photochemical inactivation -- and effects due solely to mechanical cell disruption caused by laser induced shock waves. In most of these cases, due to the laser energy densities and irradiation regions, the tissue areas exposed to shock waves of sufficient amplitude to cause damage were in close proximity to the site of laser absorption, and in these areas gross tissue damage was visible from other effects (Ref 15:201). More research is needed on this topic; however, in the area of damage to the retina, some data has been obtained.

Retinal Effects

There is no doubt that the retina is susceptible to damage from the shock wave caused by a laser pulse. Marshall (Ref 22:97-100) classified this damage into two main areas: tissue fracture induced by the passage of a strong pressure front -- a shock wave -- and tissue fracture due to stresses caused by local displacement of the affected cells. In the retina, the first type of effect manifests itself as damage to the photoreceptors in the outlying areas of the retinal lesion, while the second type of effect forms holes and tears in the nerve fibers posterior to the receptor cells. Marshall suggests that the damage to the outer segments of the receptors is indicative of a single shock front rather than a resonance effect in the tissue layer.

Pressure transients generated during laser photocoagulation as well as pulsed xenon (Xe) retinal photocoagulation

were investigated by Fraunfelder and Viernstein (Ref 23:1261-1270). This study involved the implantation of pressure transducers directly into various ocular tissues of both rabbits and monkeys. A ruby laser providing 700 μ sec pulses of 0.6 J energy caused overpressures of up to 130 torr (0.171 atm) at the point of measurement. The Xe pulses caused minimal overpressures but did cause retinal lesions. The authors stated that no evidence of ocular damage was detected from overpressures of 10 - 40 torr (0.013 - 0.053 atm) observed as a result of shock wave generation due to laser pulse absorption.

Clary and Hamrick have studied the problem of pressure transients in the eye extensively. These authors conclude that these pressure waves can definitely damage ocular tissue at or near the site of absorption, but not at distances far removed from the absorption site. They suggest, on the basis of experimental and theoretical evidence, that at the energy densities associated with threshold retinal effects, the main cause of damage, second only to direct thermal effects, is the overpressure caused by a laser induced shock wave (Ref 24:1-10).

At this time, the exact pressure amplitude of a shock wave needed to cause retinal damage has not been determined. However, the extensive laser treatment of patients by Aron-Rosa and Fankhauser has not indicated the existence of retinal damage to human patients, even after multiple laser pulse depositions in the eye, although both authors agree

that it is the action of the shock wave that destroys the posterior capsule (Ref 3;4). This is not surprising when it is realized that the plasma initiated by the laser pulse has a radius on the order of tens of microns while the retina is approximately 1.4 cm from the focal point. The small initiation volume and the comparatively distant retina enables the pressure of the shock wave to be drastically reduced in amplitude while transversing the distance from initiation site to the retina.

To see this more clearly, we turn to the treatment of a shock wave introduced by Sedov (Ref 25:238-251). In this particular treatment, the shock is reduced to a set of dimensionless variables which relate the initial energy of the laser pulse, the ambient pressure of the medium, the pressure of the leading edge of the shock, and the radius of the leading edge of the shock. A thorough discussion of these variables is included in Appendix F. If we consider an initial laser pulse energy of 10 mJ, based on this treatment, the maximum overpressure we could expect for a value at the retina would be 0.096 atm. This is based on the assumption that the laser pulse is focused in an ideal gas, with an ideal gas constant equal to 1.022.

Obviously, the vitreous is not an ideal gas, however, we can use this value as a first approximation to such overpressures as we would expect to predict and/or measure at the retina.

With this background, we can now examine the effects of

such a shock wave in terms of the overpressure present at the retina. The first step in the analysis is the development of a hydrodynamic code to predict such overpressures. Chapter IV presents this code, and the theory necessary for its derivation.

IV. Theoretical Modeling of a Shock Wave

In the Eye

Introduction

Many engineering problems exist which deal with the effects on various systems of large energy inputs into small volumes in short time intervals. Several computer codes exist which deal with the resulting shock waves which form and propagate in such systems (Ref 26; 27). The shock wave which occurs in the eye can be approximated in much the same fashion if a proper model for the eye is used. This means that if the correct ambient pressure, ambient density, and geometry for the eye is used, and more importantly, if the correct equation of state is used, a finite difference scheme can be written which allows the prediction of overpressure levels at the retina as a function of initially deposited laser pulse energy. In this chapter, the development of a one-dimensional hydrodynamic code in spherical coordinates using a Lagrangian mesh, EYESHOC, will be presented. This code is intended to yield an estimate of such overpressures.

The main objective in the development of EYESHOC is to design a code which accurately predicts the overpressure at the retina caused by a laser induced shock wave. Moreover, this must be accomplished while including simplifying assumptions which increases the ease of using the code, and decrease the required computer time. A listing of the code, the definitions of all variables involved, and a sample of

the output from EYESHOC is contained in Appendix E.

One-Dimensional Hydrodynamics Code

The following subsections present the basic equations and assumptions used to develop EYESHOC, and also include a discussion of the Lagrangian mesh which forms the coordinate system for the code.

Governing Equations

The basic equations which govern the flow of a fluid were presented in Chapter III. These are the equation of continuity, and the equations of momentum and energy conservation, Equations (1) - (3). As was discussed, an additional relation between pressure and internal energy, the equation of state, is needed to complete the set of differential equations required for the calculation of particle motions. Unfortunately, the vitreous humor is not an ideal gas, so Equation (12) is not sufficient for EYESHOC calculations. Instead, the Grüneisen equation of state is used. This equation of state is much more generally applicable, and is (Ref 18:3)

$$p = p_H + (\gamma_S/V)(E-E_H) \quad (14)$$

where

$$p_H = C^2(V_0 - V)/[V_0 - S(V_0 - V)]^2 \quad (15)$$

$$E_H = \frac{1}{2} \left[\frac{[C(V_0 - V)]}{[V_0 - S(V_0 - V)]} \right]^2 \quad (16)$$

$$\gamma_S = \gamma - 1 \quad (17)$$

$$V = 1/\rho \quad (18)$$

$$S = \frac{1}{2}\gamma \quad (19)$$

and

ρ_0 is the normal density of the material (gm/cm³)

ρ is the density (gm/cm³)

C is the speed of sound in the unshocked material (cm/sec)

Assumptions

The following assumptions were made in order to arrive at the differential equations solved by EYESHOC:

1. The local fluid velocity is dependent upon and directed along the x-coordinate in a Cartesian coordinate system, or along the r-coordinate in a spherical or cylindrical coordinate system, thereby imposing that the code be one-dimensional in nature.

2. Energy input into the code is assumed to be instantaneous, so that the addition of energy into the system is handled as an initial condition. In addition to the assumption of instantaneous temporal input, the energy is assumed to be deposited at a geometrical "point" at the center of a spherical coordinate system.

3. An artificial viscosity, q , can be introduced into the code to prevent the development of numerical instabilities which develop at a shock front due to the contraction of the material. The introduction of this variable allows for the shock to spread out, which allows for a numerical solution to the problem to exist. This is accomplished by replacing p in Equations (2) and (3) with $p+q$ where q is defined for a Lagrangian mesh as (Ref 28:313)

$$q = \begin{cases} (a\Delta r)^2 \rho (\nabla \cdot \mathbf{u})^2 & \text{if } \nabla \cdot \mathbf{u} < 0 \\ 0 & \text{if } \nabla \cdot \mathbf{u} \geq 0 \end{cases} \quad (20)$$

where

Δr is the cell size, and

a is a constant equal to approximately one-half the number of cells over which the shock is spread

4. The applicable equation of state for the calculations performed by EYESHOC is the Grüneisen equation of state. This is the correct equation because the vitreous is of sufficient viscosity to approach the properties of a solid, and this equation of state is applicable to many solids (Ref 18:3). In order to obtain a time derivative of the pressure needed to fit into the finite difference scheme of the calculation, the specific internal energy is eliminated from the equation of state as well as the rest of the

necessary differential equations. Appendix C contains the derivation. Once this has been accomplished, the resulting equation is

$$dp/dt = - \left\{ p + (\gamma-1)(p+q) - \rho^2 \rho_0 C^2 \left[\frac{\frac{1}{2}\gamma(\rho-\rho_0)\rho_0}{[\rho - \frac{1}{2}\gamma(\rho-\rho_0)]^3} \right] \right\} \nabla \cdot u \quad (21)$$

Lagrangian Mesh

The spatial mesh used in EYESHOC is defined in a Lagrangian coordinate system such that each fluid particle is labeled with a Lagrangian coordinate r which is retained as the particle moves about. The volume between adjacent mesh points is defined as a cell, and the boundaries of these cells are free to move about as necessary, but only in the positive or negative r -directions. These cell boundaries form concentric spheres in the case of the EYESHOC mesh. In essence, the boundaries in a Lagrangian mesh appear as masses connected by springs since they are free to move from point to point (Ref 16:105; 16:82; 29:14-15), where such springs would correspond to the connecting variables such as pressure, density, etc.

The overall scheme present herein is illustrated in Figure 6. Figure 6a shows the geometry of the eye, with the point of laser energy deposition identified, and the resulting shock waves graphically represented. Figure 6b shows how these shock waves would propagate in a Cartesian coordinate system, while Figure 6c gives the resulting shock wave

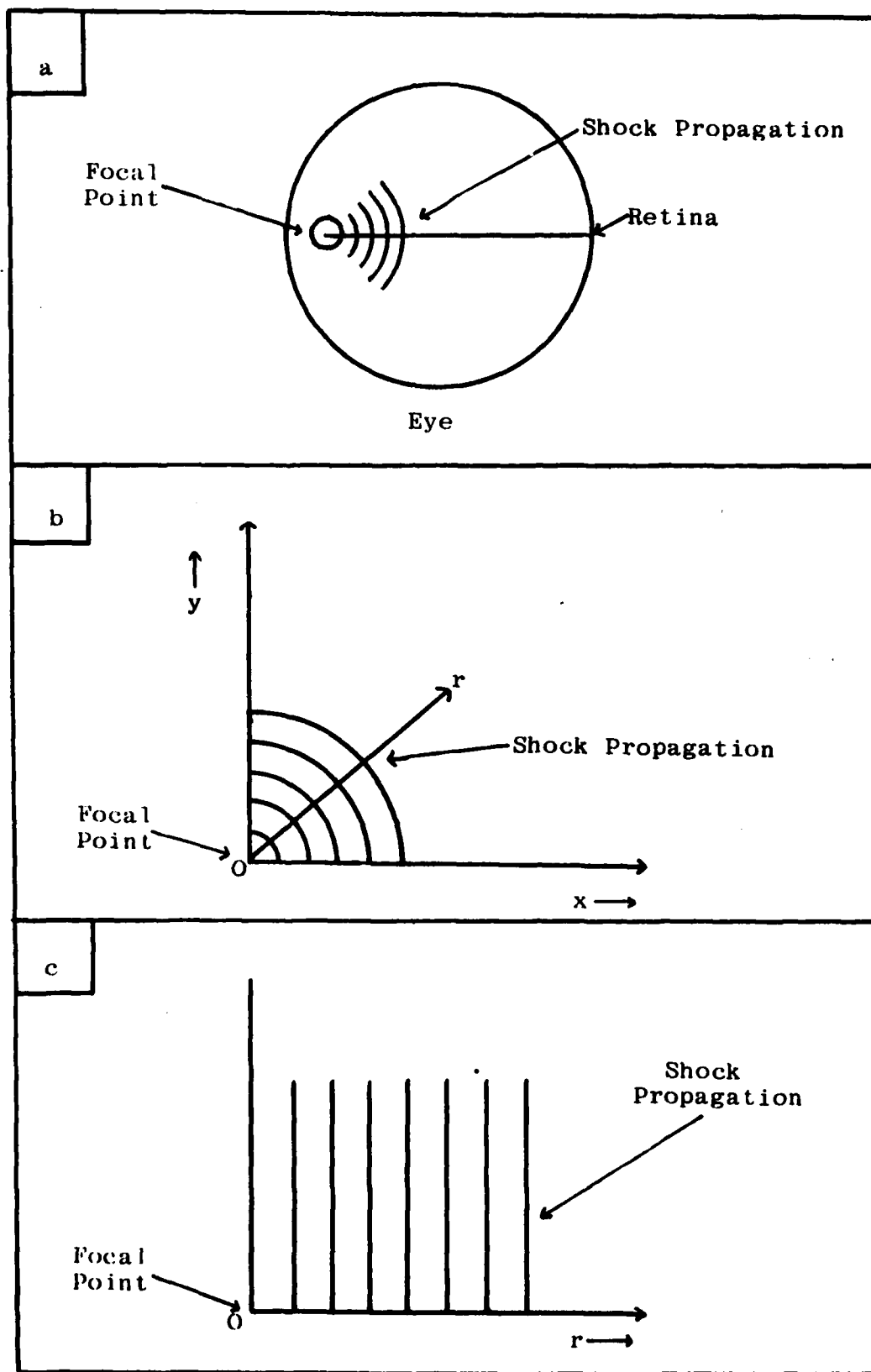


Figure 6. Lagrangian Mesh Development Scheme

propagation converted to a spherical coordinate system, thereby delineating the development of the Lagrangian mesh used in EYESHOC.

The variables appearing herein are either defined at the boundaries of the cells or at the centers of the cells. Particle velocity and position are defined at cell boundaries. Pressure, artificial viscosity, density, and specific internal energy are defined at the cell center. Figure 7 shows these quantities in the spatial mesh.

Cell	1	2	●●●	J-1	J	
Cell Boundary	r_0	r_1	r_2	r_{J-2}	r_{J-1}	r_J
Cell Boundary Velocity	u_0	u_1	u_2	u_{J-2}	u_{J-1}	u_J
Cell Centered Density	ρ_1	ρ_2		ρ_{J-1}	ρ_J	
Cell Centered Pressure	p_1	p_2		p_{J-1}	p_J	
Cell Centered Internal Energy	E_1	E_2		E_{J-1}	E_J	
Cell Centered Artificial Viscosity	q_1	q_2		q_{J-1}	q_J	

Figure 7. Lagrangian Cells and Cell Variables
Used In EYESHOC

By convention, in a Lagrangian system, the origin of the radial coordinate is chosen to be the position of the r_0 cell boundary. This is the center of the first cell at zero time.

This point is fixed, and does not vary as the positions of the cell boundaries are updated by each successive iteration of the code. It should be noted here that the cells are indeed concentric spheres, however this was not illustrated in Figure 6 in order that the variables and their relations to the cells could be shown more easily.

When dealing with hydrodynamic shock codes, an additional coordinate system could be considered, this being the so-called Eulerian mesh (Ref 18:82). In this mesh, the cell boundaries remain fixed while the fluid particles move through the mesh. The Lagrangian mesh is more accurate when dealing with a free surface, however it can become inaccurate when the cells become strongly distorted. An Eulerian mesh allows arbitrarily great distortions, however an Eulerian mesh is virtually unable to resolve the shape of a free surface. The Lagrangian mesh was considered to be the most logical choice for this thesis.

Computer Model of the Human Eye

This section will present the model of the human eye used in EYESHOC to predict overpressure levels present at the retina. The limiting assumptions will be discussed and the initial conditions which need to be determined for input into the code will be examined, as will the basic scheme of the code design.

Assumptions

The following assumptions were made in order to further

modify a standard one-dimensional hydrodynamic code as described in the earlier sections of this chapter to model shock propagation in the eye:

1. The eye is a sphere and shock waves propagating within it will also be spherical in nature, varying only in the radial or r-direction.

2. The eye is filled with a homogeneous fluid medium of density 1.007 gm/cm^3 (Ref 9:252) which has virtually the same properties as water, and can therefore be approximated as such, with the exception that the viscosity of the vitreous is much greater than that of water. From this approximation, a value of γ can be calculated. Appendix A provides this calculation, with the result that for water -- and therefore for the vitreous also -- $\gamma = 1.022$.

3. For the calculations performed by this code, reflections of the spherical shock waves will not be considered in regard to the overpressure levels at the retina. At most, these reflections will amount to an increase in the overpressure of a factor of two (Ref 15:189). For overpressure levels such as those reported in Chapter III, this is not considered to be significant. Reflections from the roof, floor, and front of the eye will therefore be ignored.

4. Posterior capsulotomies will only be modeled in patients who have had their lens removed, and who have not had a glass or plastic IOL implanted in their eye. This serves to alleviate the need to consider shock reflections from these substances, as well as the effect on the shock of

propagation into either a human lens or an IOL.

5. The distance from the posterior capsule to the retina is taken to be a nominal 14 mm.

6. All of the energy from the laser pulse is converted into internal energy for the purpose of initiating the shock wave. This energy is deposited instantaneously and the shock front develops immediately thereafter.

7. The ambient pressure of the eye is 780 torr, or 1.026 atm. This ambient pressure does not affect the nature and/or propagation of the shock wave.

Code Discussion

EYESHOC was designed as an easy-to-use analytical tool to be employed by anyone needing the type of data it can provide. The initial conditions required of the user are very few, and will be discussed subsequently. The important features of the code are as follows:

1. The code is allotted 50 spherical cells, with the origin of these cells at the center of cell one. Each cell is larger than the previous cell by a factor of 10%, i.e., r_2 equals $1.10r_1$; r_3 equals $1.10r_2$; r_4 equals $1.10r_3$, and so forth up to r_{50} .

2. Of these 50 cells, only 30 are actually needed to allow the shock to travel the distance from the posterior capsule to the retina. The remaining cells are included so that edge effects -- numerical instabilities which arise when the right-most edge of the coordinate system is en-

countered during the iterative process -- can be ignored. In its current form, the position of r_{29} is 13.4 mm, and the position of r_{30} is 14.9 mm. The value of the overpressure at 14 mm is obtained from a plot of pressure versus position at a specific time.

3. The code proceeds with the calculation in the following manner:

(a) A time step based on the local speed of sound in the medium is calculated for each cell. Appendix C provides a derivation of this time step. The minimum of each of these time steps is used as the time for the iteration.

(b) Acceleration values for each of the cell boundaries are calculated and subsequently the velocities of each cell boundary are calculated by multiplying the acceleration of the boundary by the minimum time step.

(c) New cell boundary position values are calculated by multiplying the velocity values by the minimum time step.

(d) New cell pressure, internal energy, and artificial viscosity values are calculated based on the Grüneisen equation of state.

(e) The results of that particular iteration are printed out in the form illustrated in Appendix E.

4. The code at present proceeds through 2000 iterations. Hard copy output is generated each ten iterations in the current computer system to avoid code failure due to ex-
cession of a 5000 line output line limit. If an alternate

system using EYESHOC has no such limit, hard copy output can easily be obtained for each iteration.

5. From the output generated by EYESHOC, to obtain the overpressure at the retina, the pressure p is plotted versus the position r , and a value of the pressure at 14 mm is obtained. From this value, the ambient pressure p_0 is subtracted, which leaves a value for the overpressure. This value is converted from ergs per cubic centimeter (erg/cm^3) to atmospheres (atm) by using the conversion factor

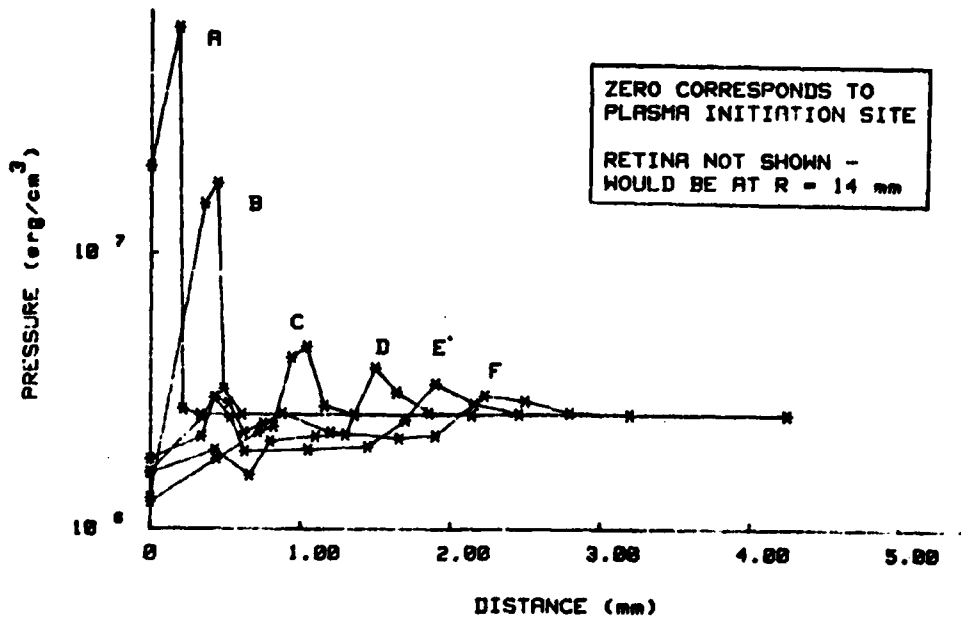
$$1 \text{ atm} = 1.01 \times 10^6 \text{ erg/cm}^3 \quad (22)$$

Several examples of pressure versus position plots at various times are illustrated in Figure 8. Plots A, B, and C reflect the shock wave nature initially present in the pressure pulse as it propagates. Plot B shows the process of "shocking-up" in which the line between the undisturbed gas and the shock wave is essentially vertical. As the wave progresses to plot C, it is beginning to relax from a true shock wave and degenerate into an acoustic pulse propagating at the local speed of sound. Plots D, E, and F also serve to illustrate this degeneration into an acoustic pulse. In essence, EYESHOC predicts that while a shock wave is present early in the propagation of the wave, prior to reaching the retina it has degenerated into an acoustic wave with the pressure of the wave greatly reduced in magnitude.

Initial Conditions

In order to use EYESHOC to predict overpressure

For an initial pulse energy at 3 mJ:



<u>Plot</u>	<u>Velocity (cm/sec)</u>	<u>Time (sec)</u>
A	3.56×10^5	6.85×10^{-8}
B	2.03×10^5	2.46×10^{-7}
C	1.61×10^5	6.83×10^{-7}
D	1.53×10^5	1.01×10^{-6}
E	1.50×10^5	1.30×10^{-6}
F	1.48×10^5	1.55×10^{-6}

Figure 8. Pressure Versus Distance for Various Times

levels at the retina, only the specific internal energy and pressure values for the first cell need to be calculated and inserted into the code by the user. Appendix D provides a sample calculation of these values, and Table I lists the first cell specific internal energy and pressure values which were used in the three test runs conducted with the code. While these values are a function of cell size, it was assumed that the main variable of interest was the pulse energy and that this energy was spread uniformly over the entire first cell so that in essence, the cell size is not of consequence. This dependence on pulse energy is also seen in the treatment of Sedov (Ref 25:238).

TABLE I
EYESHOC First Cell Specific Internal Energy
and Pressure Values for Test Runs

Pulse Energy (mJ)	Internal Energy (erg/gm)	Pressure (erg/cm ³)
3.75	8.89×10^9	1.97×10^8
7.50	1.78×10^{10}	3.93×10^8
22.50	5.33×10^{10}	1.18×10^9

Code Validation

In an effort to accurately establish the validity of EYESHOC, the results obtained for an ideal gas with a value of γ equal to 1.4 were compared with the results obtained by Sedov (Ref 25:247-248) for the identical case. The results

of this investigation are discussed in detail and presented in Appendix G.

Figure 9 shows the relationship between two dimensionless ratios defined by Sedov. The ratio p_2/p_1 refers to the ratio of the maximum pressure of the shock to the ambient pressure while the ratio r_2/r^0 refers to the ratio of the radial distance at the point of maximum pressure to a constant dependent upon the initial laser pulse energy and the ambient pressure of the medium. For the values used in this thesis, r^0 varied from 0.33 cm to 0.60 cm and the ratio of r_2/r^0 for the experimental distances to be discussed in Chapters V and VI varied from 1.1 to 4.3. For those values, the plot of p_2/p_1 versus r_2/r^0 predicts a radial dependence of $1/r^{0.5}$ for $\gamma = 1.022$ and $1/r^{0.06}$ for $\gamma = 1.4$. However, it must be noted that this is an order of magnitude change in the radial dependence and is entirely due to the γ scaling present in the theory of shock waves. If the value of γ for water calculated for this thesis is slightly wrong, it could change the plot in Figure 9 by a wide margin. The most important point to note is that the radial dependence is decreasing as the pressure drop becomes less and less significant. This is indicative of the great drop in pressure as the shock wave degenerates into an acoustic pulse and loses much of its initial radial dependence.

Predicted Results

As shown above, three test runs were made using the

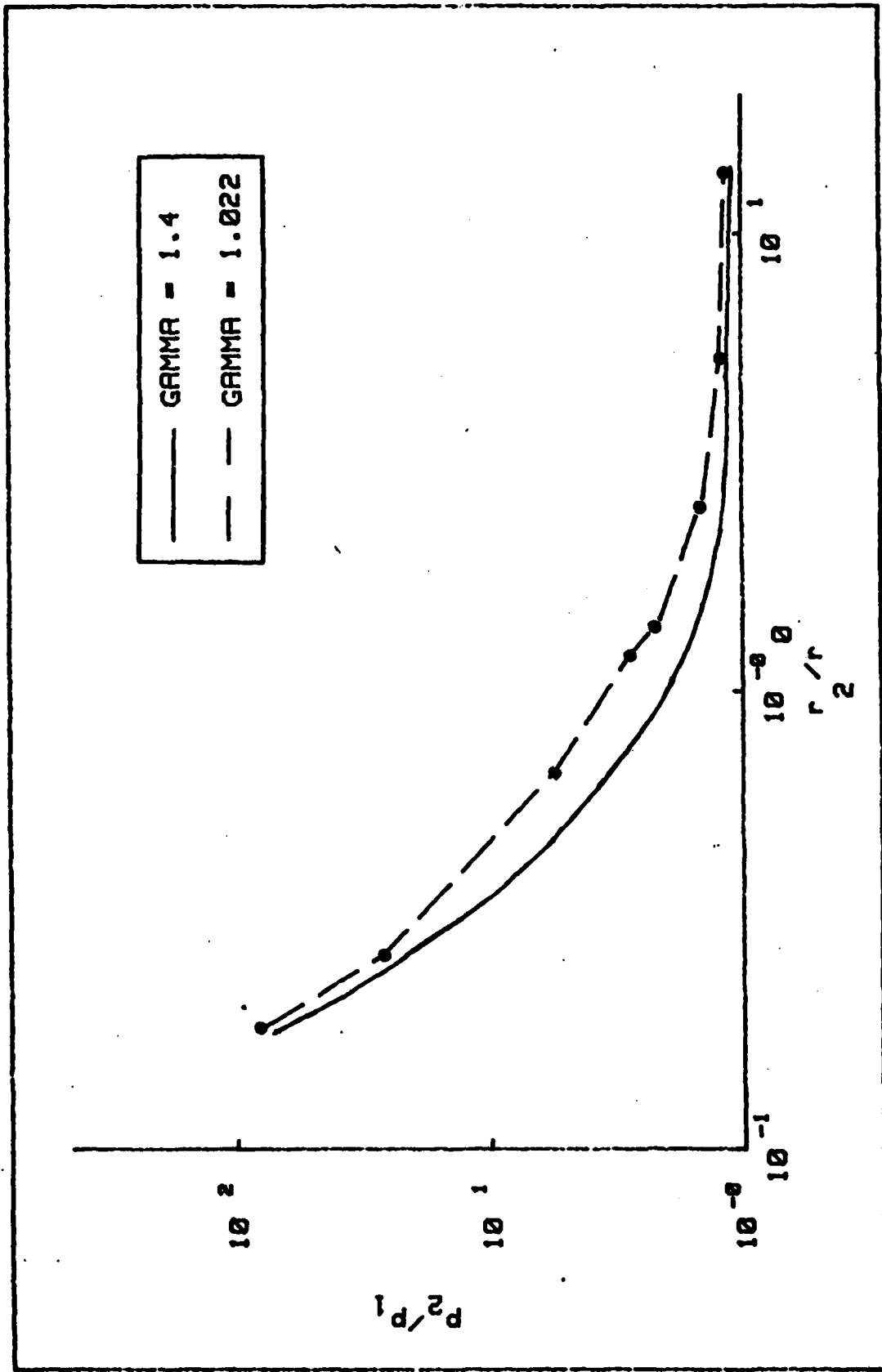


Figure 9. Pressure Drop Across Front Versus Shock Wave Radius

EYESHOC code, with energies of 3.75 mJ, 7.50 mJ, and 22.50 mJ at the focal point. The overpressure level at a distance of 14 mm from the point of laser energy deposition was determined in the manner previously discussed, and the predicted values of the overpressures at the retina are listed in Table II.

TABLE II
Predicted Overpressures at the Retina for
EYESHOC Test Runs

Pulse Energy (mJ)	Overpressure ($\times 10^{-2}$ atm)
3.75	1.8
7.50	3.6
22.50	11.0

We now have overpressures predicted based on the theoretical modeling of a shock wave in the eye. While the actual measurement of overpressures in an eye is beyond the scope of this thesis, we will now discuss the test system used to model an ocular system, and the overpressures measured by this experimental arrangement.

V. Experimentation

At this point, the main thrust of this thesis moves from theoretical predictions to experimental investigations. This chapter will present the materials employed and the procedures followed in an effort to obtain measured overpressure levels caused by laser induced shock waves. With the values of overpressure levels listed in Table II and those reported in Chapter III, the need was great to attempt to validate the predictions of EYESHOC experimentally. The following describes how this was accomplished.

System Design

The discussion of the experimental system used in these experiments will be subdivided into discussions of the laser system, the pressure transducer and associated electronics, and the test cell and vitreous model. Figure 10 provides a schematic drawing of the overall system while Figure 11 is an actual photograph of the system during its use.

Laser System

The laser system used in this study was an entirely self-contained Q-switched or mode-locked Nd:YAG laser, assembled by Quantel International. The laser is water-cooled, and emits monochromatic pulses of wavelength equal to 1064 nm. The laser radiation is coupled to an ophthalmic slit lamp via an articulated arm, which was assembled by American

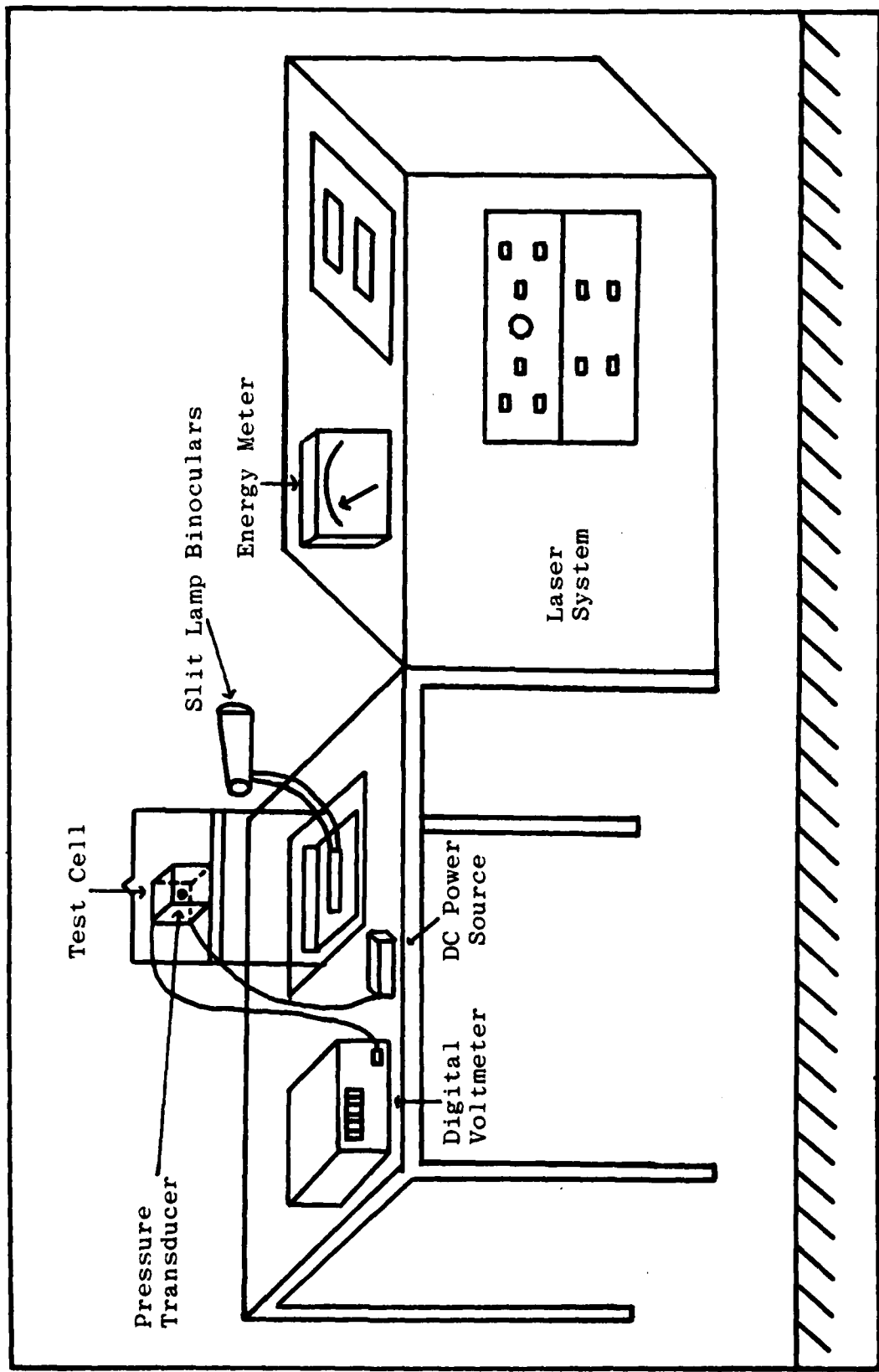


Figure 10. Test System Schematic



Figure 11. Test System Photograph

Medical Optics, Incorporated, so that the output of the overall laser system is at the rear of the slit lamp binoculars, and can be focused into a patient's eye. In addition to the Nd:YAG radiation exiting the system, the laser houses a helium-neon (He-Ne) alignment laser and a visible light beam. The internal optics are adjusted so that all three beams can be focused simultaneously, i.e., if the visible beam and the He-Ne alignment beam are in focus, the point of their focus is the point of focus of the Nd:YAG laser also. The slit lamp binoculars feature a filter for both the He-Ne and Nd:YAG beams to prevent injury to the ophthalmologist during the laser assisted psoterior capsulotomy.

The Q-switch apparatus of the laser will be examined in detail. However, the mode-locking mechanism of the laser

system will not be discussed, since no experiments were conducted for this thesis using the laser system in the mode-locked operating mode. Figure 12 provides a schematic of the interior of the laser cavity itself, with a list of the optics contained therein.

In the Q-switched mode the laser emits 15 nsec pulses of varying energy levels ranging from 1 mJ to 35 mJ. The beam is near diffraction limited with a 0.7 mrad half-angle beam divergence. The cavity is formed between a flat 100% reflecting mirror and a convex 100% reflecting mirror with radius of curvature of 3 m. These are items 1 and 9 respectively in Figure 12. To insure Q-switched operation, the turning prism, item 5, must be inserted into the beam path.

The free running mode of the laser is suppressed by the intra cavity quarter-wave plate, WP-1. This element ensures a 90° rotation of the beam on a double pass and subsequent rejection of this mode by the adjacent Glan-Taylor polarizer. Lasing in the Q-switched mode occurs when a quarter-wave voltage is impressed across the Pockels Cell, item 2, which further rotates the beam by 90° . This restores the beam to the horizontally polarized state, and it propagates to the laser rod for amplification. The beam undergoes a double pass through the quarter-wave plate WP-2, and upon returning to the second Glan-Taylor polarizer, the vertical component of the beam is diverted and used as the laser output. The horizontal component of the beam continues to the Q-switch leg of the path to sustain oscillation in the cavity

(Ref 30:3-5).

The laser was operated via a footswitch which enabled the user to fire the laser at will. In addition, the laser has the capability of operating at a repetition rate of 10 Hz, for test purposes. When testing the laser, a turning mirror is brought into the beam so that the pulses can be focused into a Quantel Energy Meter head and the laser output can be read on an analog scale permanently attached to the laser system itself.

This laser system was the prototype for a marketable system currently available from American Medical Optics, Inc. The laser was made available for use in this study by Dr. Richard H. Keates, Professor of Ophthalmology, of the Ohio State University Eye Clinic. All tests were performed at the Ohio State University.

Pressure Transducer and Associated Electronics

The pressure transducer used in these experiments was a Kulite Semiconductor Pressure Transducer, Model Number VQH-250-5. A photograph of the transducer is included in Figure 13. The transducer was a gage type, consisting of a Wheatstone bridge circuit with an input impedance of 2971 ohms and an output impedance of 2505 ohms. The transducer was rated for a pressure of 5 pounds per square inch (psi) (14.7 psi = 1 atm), with a maximum pressure of 20 psi.

Physically, the transducer has an outside diameter of 6 mm and is 63 mm long overall. It consists of a barrel 17 mm

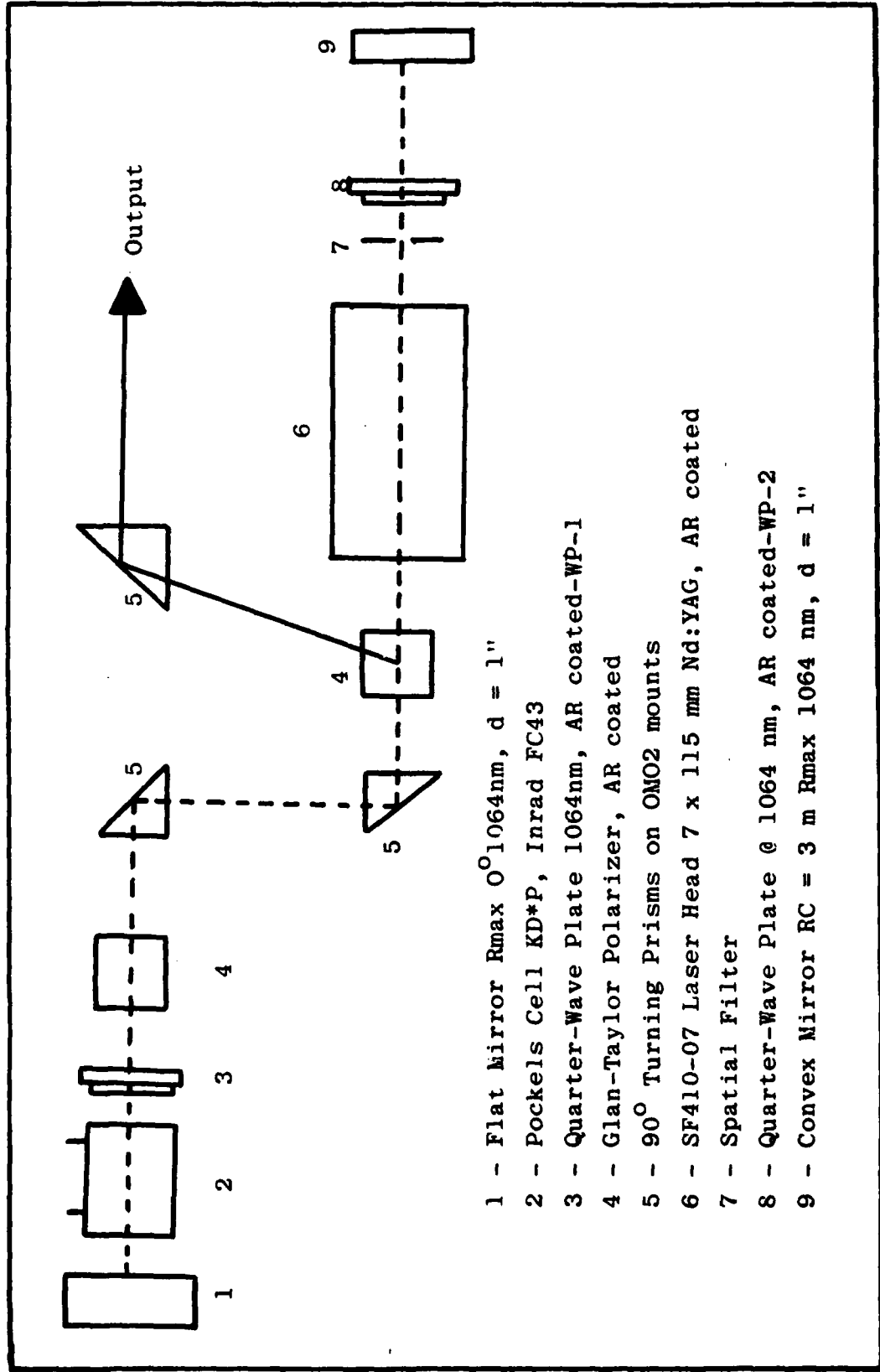


Figure 12. Laser Oscillator Schematic (Ref 30:5)

long and a nozzle attached to the rear of the barrel 46 mm in length. A diaphragm is located inside the barrel of the transducer. This diaphragm undergoes a translation when a pressure pulse is applied to the transducer. The movement of this diaphragm then alters the resistance in one leg of the bridge circuit, which is eventually read out as the output of the transducer. The transducer was calibrated to a sensitivity of 11 mV/psi, so that an overpressure of magnitude equal to 1 psi reaching the diaphragm would cause an 11 mV signal to be generated by the bridge circuit. This signal could then be detected by an oscilloscope, or as was used in this study, by a digital or analog voltmeter.



Figure 13. Pressure Transducer

The power supply for the transducer consisted of an Eveready BA-53 dry cell in series with a 500 ohm variable

resistor. This type of voltage source was used in order that the 20 V DC excitation voltage which was used as the calibration parameter for the transducer could be maintained at a stable level. In addition, the use of a dry cell as a voltage source decreases the overall noise level of the system, which would have been greater had the voltage source been a conventional line DC power supply. The dry cell and variable resistor were housed in an aluminum shield to further lower the noise level, and the voltage from the dry cell to the transducer was delivered via shielded cable using BNC type connections.

The output of the transducer was measured using a Data-Precision 3500 Digital Voltmeter. The voltmeter was used in a mode such that the minimum detectable voltage was 0.1 mV. The transducer was also housed in an aluminum shield, which was affixed to the rear of the test cell, with the barrel of the transducer entering the test cell through a hole bored in the back wall of the cell. The output of the transducer was connected to the voltmeter again via shielded cable using BNC type connections.

Test Cell and Vitreous Model

The experiments conducted in this study employed a glass and plexiglas test cell developed by J. Riggins (Ref 5:57). The cell is illustrated in Figure 14. The cell was constructed of plexiglas on the sides, top, and bottom, while the two faces

-- front and back -- in the path of the beam were constructed of glass. The top of the cell was removable to allow the cell to be filled with various substances for testing purposes. The lid was also slotted to allow for the translation of a small plexiglas cylinder, which was used to aid in the assignment of distances from the transducer. The slide which moved the cylinder was kept under tension by two springs while movement was obtained by a fine threaded screw which provided movement of 0.625 mm per rotation.

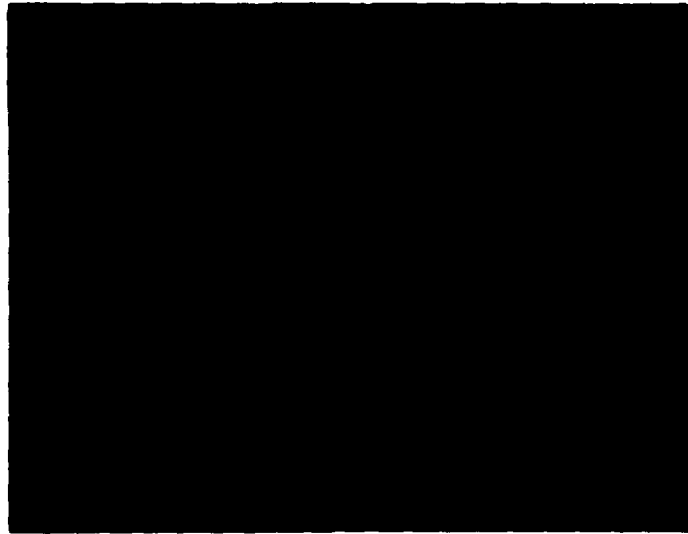


Figure 14. Test Cell

For this study, the test cell was filled with balanced salt solution (BSS). This solution had previously been shown

to have approximately the same breakdown characteristics of the vitreous itself (Ref 5:85). Actual vitreous was originally to have been employed for testing purposes, however human vitreous in the quantities needed -- 50 ml per test -- was virtually unobtainable. The use of hog vitreous was considered, however the material obtained was not of sufficient purity to lend credence to any measurements which could have been generated.

The overall dimensions of the test cell were 40 mm high by 40 mm wide by 32 mm deep. These dimensions yield a volume of 51.2 ml for the test cell. As was mentioned, the front and back of the cell were constructed of glass. The glass front of the cell was removed in order to determine the absorption of the laser radiation due to the glass itself. The glass was placed in a Perkin-Elmer Model 350 Spectrophotometer, and a plot of transmittance versus wavelength from 0.6 to 2.7 microns was generated. This plot is shown in Figure 15. To identify the Nd:YAG laser wavelength absolutely, a Laser Optics narrow-bandpass filter selectively coated with a 100 angstrom (\AA) coating for 1.06 microns was used. The results of this investigation revealed that 75% of the incident radiation at 1.06 microns was being transmitted to the interior of the cell. Using this data, all laser pulse energies were corrected for this factor in subsequent uses.

The laser system, the pressure transducer, and the test cell filled with balanced salt solution were integrated into

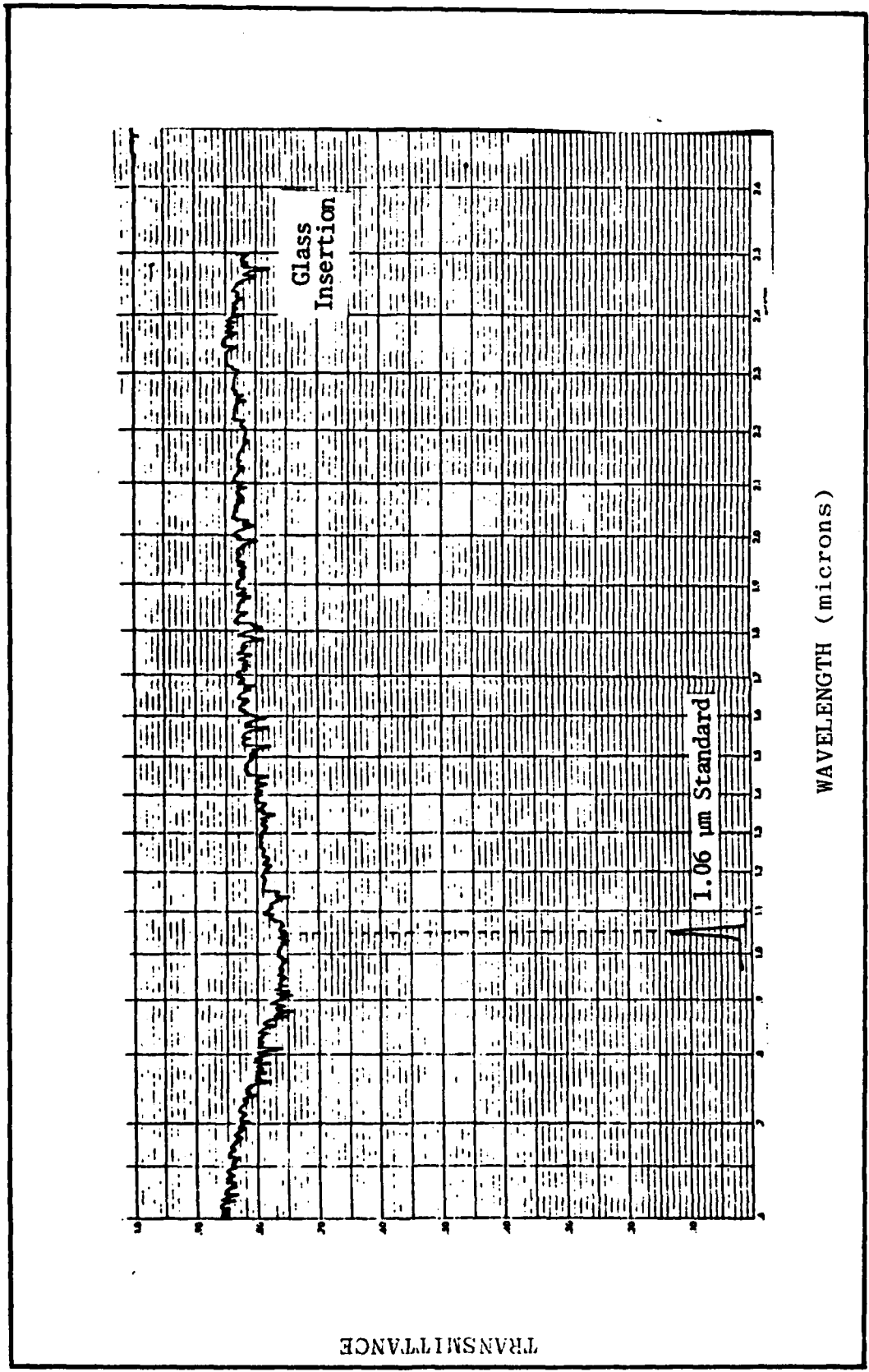


Figure 15. Cell Front Transmission Data

a total test system for the determination of the laser induced shock wave overpressures at specific distances from the diaphragm of the transducer. Figure 16 is a close-up of the test cell with the transducer attached to the rear of the cell. The entire cell-transducer assembly is attached to the output end of the laser system for actual experimentation.

Experimental Procedures

Once the equipment was assembled, the following steps were performed in order to determine the overpressures caused by several laser pulse energies at varying distances from the pressure transducer:



Figure 16. Test Cell with Attached Pressure Transducer

1. The output of the laser was diverted into the energy meter head, and the pulse energy was set to a value of 5 mJ. Subsequent tests were conducted with pulse energies of 10 mJ, and 30 mJ, as recorded using the readout of the energy meter. Making use of the 75% transmission factor, these values correspond to pulse energies at the focal point of 3.75 mJ, 7.50 mJ, and 22.50 mJ, respectively.

2. The output of the laser was again allowed to enter the test cell. The translating cylinder was initially set at a distance of 14 mm from the transducer, but was moved to distances of 10 mm, 8 mm, and 6 mm from the transducer in subsequent experiments.

3. Ten laser pulses were focused at the distances mentioned above, and the overpressure induced by each was measured using the digital voltmeter. The average overpressure for each energy and distance combination was determined by calculating the mean of the ten values, and the error in the measurements was calculated by determining the standard deviation of each of the mean values. The distances were determined to within ± 1 mm using the translating cylinder, the slit lamp binoculars, and the spark which is visible upon breakdown of the BSS. It should be noted that each of the ten pulses focused into the test cell initiated breakdown of the BSS.

4. After each energy and distance combination had been tested, the test cell was re-filled with fresh BSS to prevent the accumulation of any possible artifacts created in the

breakdown process. This was done to maintain as much continuity in the measurements as possible.

This concludes the discussion of the test system, and the manner in which the tests were conducted. The next chapter provides the results obtained in these experiments and compares these results with those predicted by theory.

VI. Results and Discussion

This chapter will present the overpressure measured in the experiments described in Chapter V and compare these values to the predictions given in Chapter IV. In addition, the results will be examined in order to determine whether or not they fit the model of a spherical shock wave with reference to pressure versus energy and pressure versus distance.

Overpressure versus Energy

The overpressures measured at the transducer for varying distances from the transducer as a function of input pulse energy are listed in Table III. It can be seen that overpressures ranged from 0.018 atm to 0.432 atm, or changes in the overall pressure at the transducer of 1.7% and 42.1% respectively. If the values obtained for a distance of 14 mm are examined, it can be seen that the maximum overpressure was 0.077 atm, or an overall change of 7.5% from ambient pressure. If the BSS test cell environment is a valid substitute for the eye, which we believe it to be, then these would be the overpressures expected during the posterior capsulotomy procedure. It is very important to note that the largest input pulse energy did not alter the pressure by more than 10% at this distance.

Based upon theoretical treatments such as by Sedov the overpressure should be linear when plotted versus the

input pulse energy. Figure 17 is a plot of the values listed in Table III, for each distance from the transducer. The correlation coefficient was calculated for each of the lines, with the result being that each of the four lines plotted in Figure 17 had a correlation of 0.999 or greater. A perfect correlation between data points would yield a correlation coefficient equal to one, hence it is obvious that the overpressures measured in this study are indeed linear with the pulse energy, as expected.

Overpressure versus Distance

Based on the degeneration of the shock wave into an acoustic pulse the expected variation of the overpressure with distance from the laser induced breakdown site to the transducer is for the overpressures to show a $1/r^2$ fall-off as the distance increases. In view of this, if the overpressures are plotted versus the distance, to accurately show this type of trend, we should multiply the overpressures by the square of the distances.

The values of the overpressures obtained versus the distance from the transducer are listed in Table IV. In addition, these values are plotted in Figure 18, which gives three plots of overpressure times distance squared versus distance, one plot for each of the three energies tested. As is noted on the figure, the broken line indicates the measured values, while the solid line indicates the results of a least-squares fit analysis of the data. As can be seen, the values obtained

TABLE III
 Overpressures versus Energy Deposited at Focal Point
 for Varying Distances from Retina

E (mJ)	R = 6 ± 1 mm	R = 8 ± 1 mm	R = 10 ± 1 mm	R = 14 ± 1 mm
	P (x 10 ⁻² atm)			
3.75	8.8 ± 0.7	6.2 ± 0.6	2.9 ± 0.5	1.8 ± 0.3
7.50	16.8 ± 1.0	9.2 ± 0.6	5.8 ± 0.6	3.1 ± 0.4
22.50	43.2 ± 1.1	23.1 ± 1.9	16.3 ± 0.8	7.7 ± 1.2

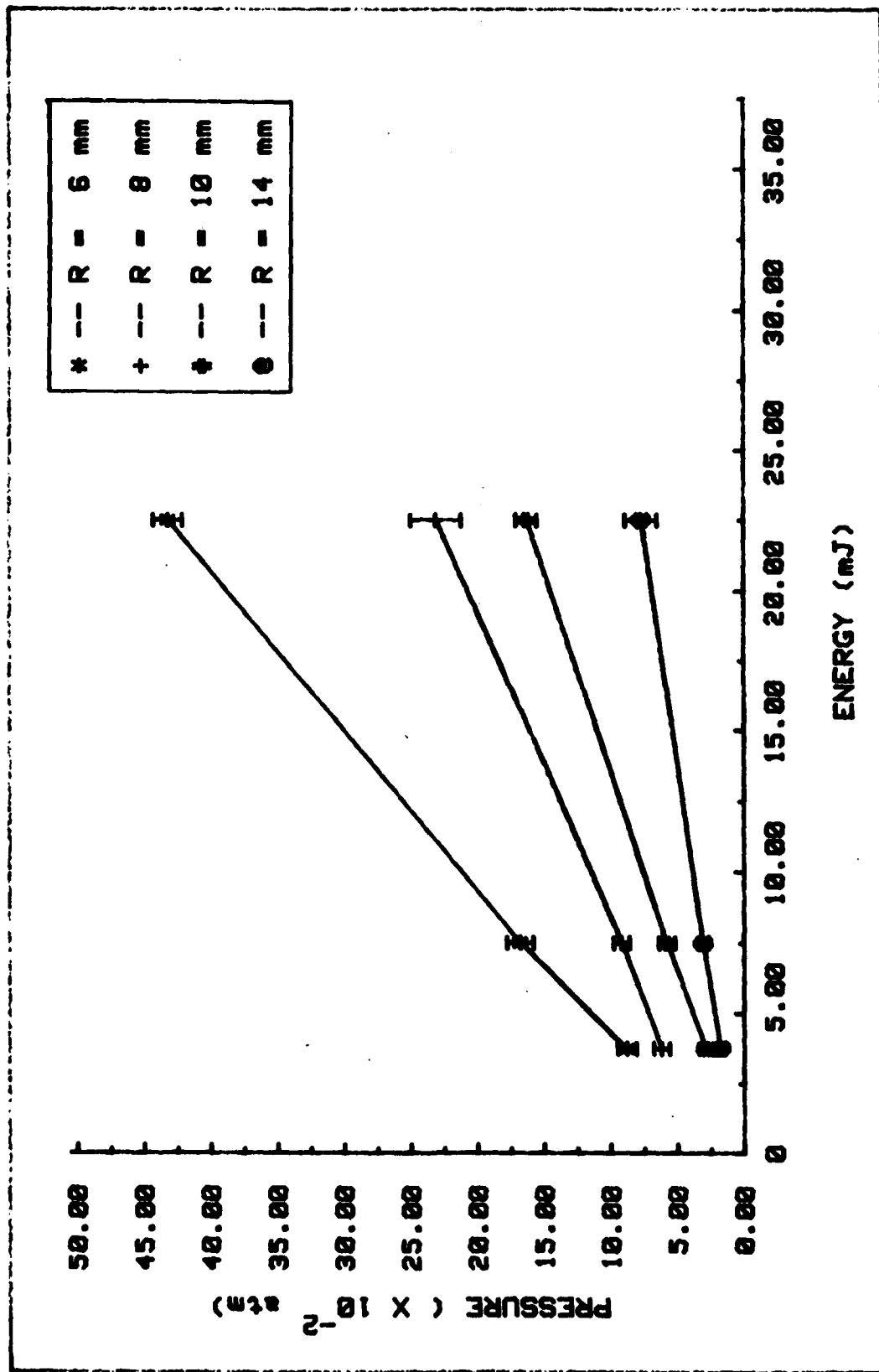


Figure 17. Overpressure versus Energy

in the least-squares analysis are virtually linear, as is expected based on the increase in energy. That is, the value for $E = 22.75$ mJ is approximately six times the value for $E = 3.75$ mJ. From the graphical plots in Figure 18, it seems indeed safe to conclude that the pressure does show a $1/r^2$ fall-off with distance.

Comparison of Predicted versus Measured Overpressures

The magnitudes of the measured and predicted overpressures, and the percent change from ambient pressure which they represent are listed in Table V. The differences in measured and predicted variations from ambient pressures can be seen to be less than 5% in each case -- assuming the worst case analysis in which the lower range of the standard deviation is used as the value for the measured overpressures. These values represent the maximum pressure levels present in an acoustic pulse propagating at the local speed of sound. It should be noted that these values are for the breakdown-to-transducer distance of 14 mm only. The values listed in Table V are plotted in Figure 19.

If the trends exhibited in Figure 19 are analyzed closely, it can be seen that the difference between the two lines increases as the energy increases. This is an indication of a discrepancy occurring in either the code, the measurements, or possibly in both. If the plot is examined closely, it can be seen that the line indicating the predicted overpressures is completely linear, while the line

TABLE IV
Overpressures Times Distance Squared for Varying
Energy Levels at Focal Point

R (mm)	R ² (mm ²)	E = 3.75 mJ	E = 7.50 mJ	E = 22.50 mJ
		PxR ² (atm-mm ²)	PxR ² (atm-mm ²)	PxR ² (atm-mm ²)
6	36	3.17 ± 0.25	6.05 ± 0.36	15.55 ± 0.40
8	64	3.97 ± 0.38	5.89 ± 0.38	14.78 ± 1.22
10	100	2.90 ± 0.50	5.80 ± 0.60	16.30 ± 0.80
14	196	3.53 ± 0.59	6.08 ± 0.78	15.09 ± 2.35

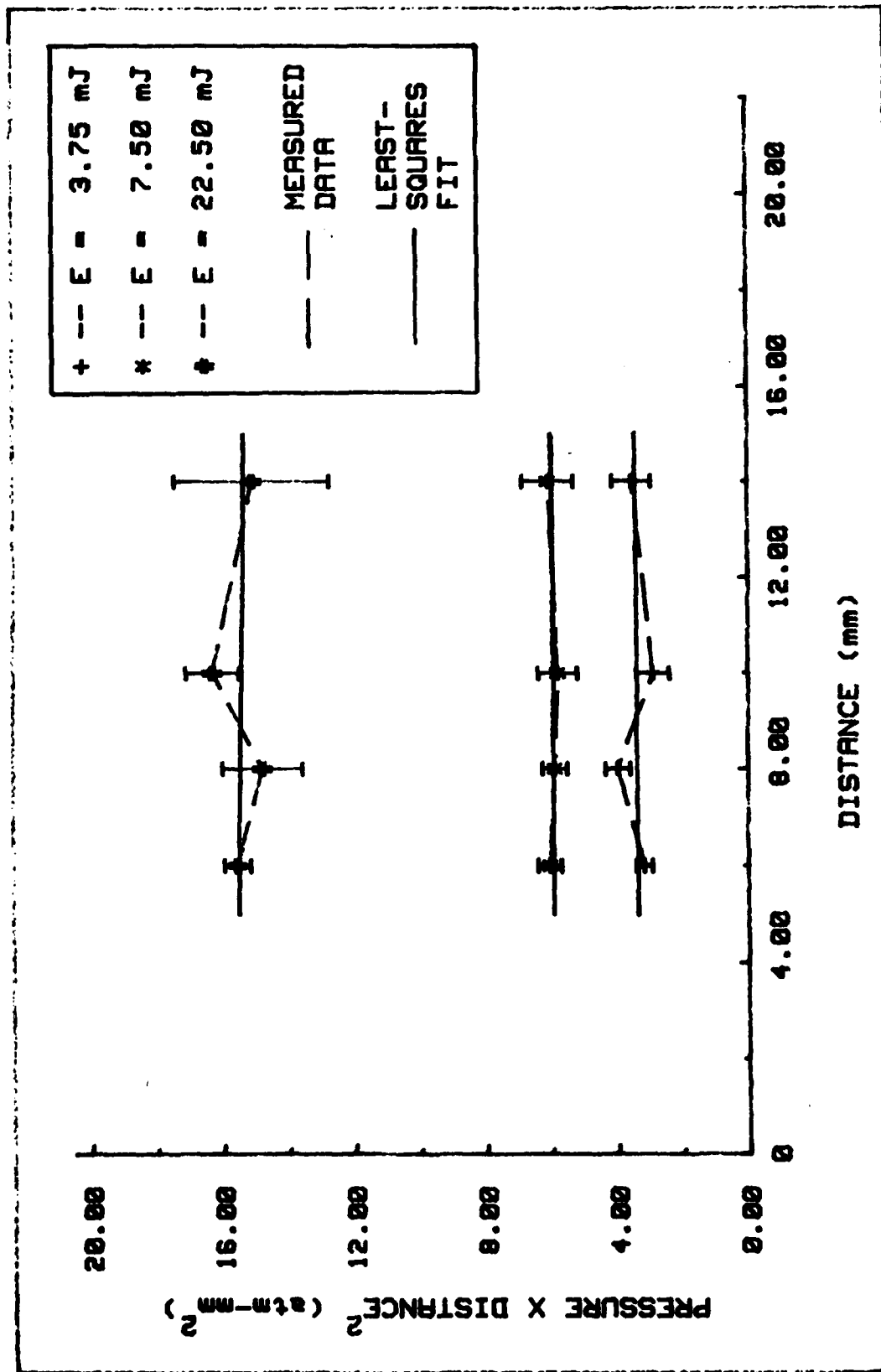


Figure 18. Overpressure Times Distance Squared versus Distance

TABLE V
 Comparison of EYESHOC Predictions and
 Measured Overpressures

Energy (mJ)	Overpressure ($\times 10^{-2}$ atm)		Percent Change from Ambient	
	Predicted	Measured	Predicted	Measured
3.75	1.8	1.8 ± 0.3	1.7	1.7 ± 0.3
7.50	3.6	3.1 ± 0.4	3.5	3.0 ± 0.4
22.50	11.0	7.7 ± 1.2	10.7	7.5 ± 1.2

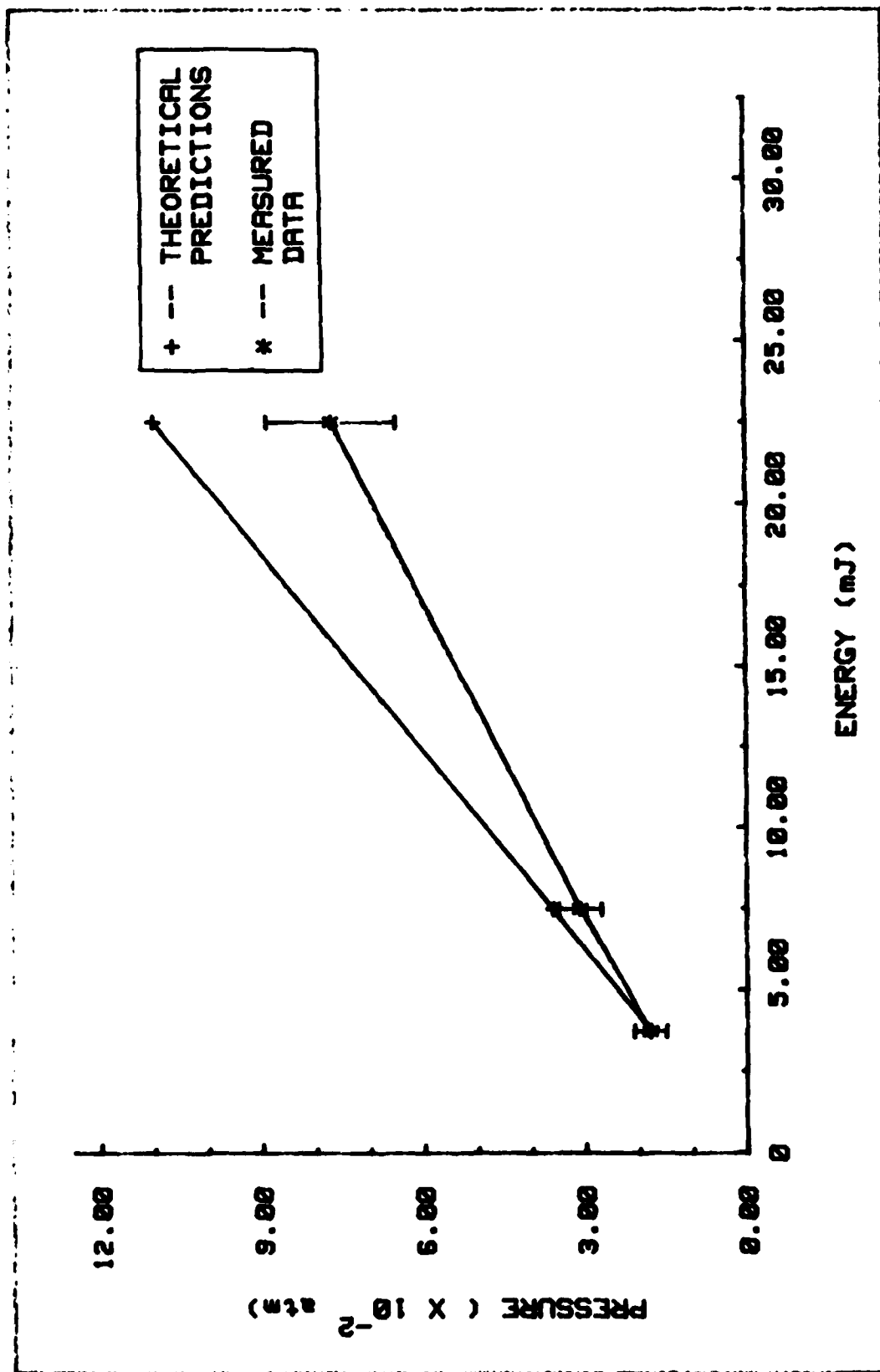


Figure 19. Comparison of Predicted and Measured Overpressures

indicating the measured overpressures begins to show a fall-off from its original slope, thereby deviating from total linearity as the energy of the pulse increases. However, if the deviation of the measured values is considered, it can be seen that for $E = 7.5$ mJ, the predicted value lies in the range of the measured value and for $E = 22.50$ mJ, the difference between the largest measurement and the predicted value is only 0.011 atm, which is a miniscule difference. At the levels of overpressures being discussed in this thesis, such differences cannot be considered significant. The measured values for this case are deemed quite good, in view of the fact that at the greatest pulse energy, the greatest deviation between the values yields a difference of 4.4% in the percent change from ambient.

This concludes the presentation and discussion of the results obtained in the experimental portion of this investigation. At this point, we have examined the theory associated with both the ocular system in humans and the physics of shock waves; we have derived a theoretical hydrodynamic code for predicting laser induced shock wave overpressures at the retina; and we have developed and implemented a test system designed to measure such overpressures. All that remains is to assemble the data generated from both the analytical and experimental portions of this study and draw conclusions from it. This is the topic of Chapter VII.

VII. Recommendations and Conclusions

The purpose of this chapter is to analyze the findings in this study from an overall point of view. We wish to examine what the study has accomplished, and recommend further investigations in the area of Nd:YAG laser-assisted ocular surgery. In addition, clinical conclusions will be presented in this chapter which can be used as possible guidelines for the ophthalmologist when performing posterior capsulotomies with Nd:YAG lasers.

This study examined the shock wave generated in the posterior chamber of the human eye during posterior capsulotomies performed with Nd:YAG lasers. These shock waves were modeled using a one-dimensional hydrodynamic code in spherical coordinates utilizing a Lagrangian mesh. The code predicted that the shock waves initially present degenerated into acoustic pulses prior to reaching the retina and that the overpressures at the retina are less than 0.15 atm. In addition, overpressures caused by Nd:YAG laser systems currently used by several ophthalmologists to treat patients were measured in a test chamber containing balanced salt solution. These measurements were made for varying distances from the point of energy deposition to the pressure transducers, as well as for varying input laser pulse energies. The overpressures measured in this experiment varied from 0.018 atm to 0.432 atm. A comparison of predicted overpressure values obtained from the code and measured overpressure values obtained from

the experiments indicated a high degree of agreement between the two methods of generating the overpressure at the retina during this type of ocular surgery.

Further studies and experiments are necessary for a complete understanding of the processes involved when the energy from a Nd:YAG laser is focused into the posterior chamber of the eye. Such studies should include both additional experimental and theoretical investigations. To this end, changes are proposed for the shock code and future experiments are suggested.

Shock Code Limitations and Proposed Changes

1. This thesis was concerned exclusively with the retina in terms of the effects of the shock wave. Analytical predictions such as those obtained from EYESHOC should be extended to other possibly sensitive portions of the eye to determine the overpressures at these tissues. Examples include the iris, cornea -- assuming no lens present -- or the lens itself. This would be a simple calculation based on the results presented in this study if the distances from the point of laser energy deposition to the tissues of interest were known. These calculations should be made, and subsequent codes devised to determine their accuracy.

2. Unfortunately, EYESHOC suffered from some inherent numerical instabilities which survived all efforts to remove them. Such instabilities are not totally uncommon in codes

of this type (Ref 29:34-66), however with extensive work they can be reduced and/or eliminated altogether. The primary aid in reducing instabilities is through the use of artificial viscosity, q , which is designed to smooth out the shock front and prevent such instabilities. More extensive analysis of the artificial viscosity present in the code should be performed.

3. Finally, an effort should be made to incorporate the actual viscosity of the vitreous into the analytical model designed for EYESHOC. The vitreous is four times as viscous as water (Ref 9:252), but this does not appear in the model, which is based almost exclusively on water. This could possibly appear in relation to the density, however this author offers no suggestion as to the manner of incorporation.

The three points listed herein should be the topics of future theoretical analyses. However, it cannot be overlooked that the results of EYESHOC are in very close agreement with the overpressures obtained in experimental studies, both by other experimenters and those accompanying this thesis effort. In view of this, it must be concluded that EYESHOC is a useful tool for predicting the overpressures associated with the Nd:YAG laser procedure, and in this respect, EYESHOC accomplishes its intended purpose.

Future Experimentation

The experiments conducted in this thesis, as well as

those discussed in Chapter II lay a firm experimental foundation needed to characterize Nd:YAG laser assisted posterior capsulotomies. However, future experiments are necessary and should be of two main types, in vivo and in vitro studies.

Initially, the next group of experiments should be performed in an in vitro manner, i.e. with a test cell and vitreous model as was used in this thesis. However, two main changes should be instituted in these studies. First, the test cell should be altered in geometry so that it is the same size and shape as an actual eye. This cell should be fitted with multiple pressure transducers rather than the single transducer used in this study. This would enable overpressure measurements to be obtained for areas of the eye in addition to the retina. Second, a substance other than BSS should be used for the vitreous model. This will involve preliminary experimentation to identify a suitable model for the vitreous which not only exhibits the same breakdown characteristics, but is approximately of the same viscosity as the vitreous. These two changes would enable the closest correlation between a test system and an actual patient to be achieved.

Subsequently, experiments should be undertaken in vivo with both rabbits and monkeys, to measure the overpressures generated in living systems. As mentioned above for test cell studies, multiple pressure transducers should be implanted in these animals, and values of the overpressures

should be determined at all possible points in the eye. To totally investigate the effects of such shock waves, electron microscopy should be performed on all ocular tissues from the animals irradiated in the manner discussed in this thesis.

Finally, these same studies should be conducted on human eyes which have been obtained from an eye bank. This would of course simulate the actual conditions present during a posterior capsulotomy as closely as possible.

Clinical Conclusions

The most important goal of this thesis was to develop guidelines for the ophthalmologist to use when performing a posterior capsulotomy on a patient with regard to the overpressure at the retina caused by a laser induced shock wave. To this end, we have determined the values of such overpressures, and now define a maximum overpressure which should not be exceeded.

Based on the results obtained in this thesis, a maximum level of acceptable overpressure of 0.10 atm is proposed as the treatment threshold when performing posterior capsulotomies with Nd:YAG lasers. This value would allow laser pulses of up to 10 mJ to be used with no ill effects. These pulses should be of nanosecond pulsewidth, as were those employed in this study. In addition, this overpressure level will allow for pulse energy deposition as far as 6 mm behind the posterior capsule without damage to the retina.

This would enable the ophthalmologist to utilize the Nd:YAG laser in the removal of vitreous bands as well, without retinal damage concerns.

One of the primary reasons for assigning the 0.10 atm level as the maximum acceptable overpressure deals with the current use of Nd:YAG lasers by practicing ophthalmologists. Several thousand patients have undergone posterior capsulotomies performed by doctors Keates, Fankhauser, and Aron-Rosa, and not one patient has suffered retinal damage attributable to a laser induced shock wave or acoustic pulse. The lasers used by these doctors all meet the criteria set forth above, i.e., pulses of less than 10 mJ, nanosecond pulsewidths, and distances to the retina normally greater than 10 mm during a posterior capsulotomy procedure. With these limitations met, an ophthalmologist could perform this type of procedure without fear of patient injury.

Bibliography

1. Kirsch, Ralph E. "Intraocular Lenses - The Conservative Approach," Controversy in Ophthalmology, edited by Robert J. Brockhurst, et. al. Philadelphia, London, and Toronto: W. B. Saunders Co., 1977.
2. Dorell, E. D. Surgery of the Eye. London: Blackwell Scientific Publications, 1978.
3. Aron-Rosa, D. et. al. "Use of the Neodymium:YAG Laser to Open the Posterior Capsule After Lens Implant Surgery: A Preliminary Report," Journal of the American Intraocular Implant Society, 6 (4): 353-354 (October 1980).
4. Fankhauser, Franz, et. al. "Clinical Studies on the Efficiency of High Power Laser Radiation Upon Some Structures of the Anterior Segment of the Eye," International Ophthalmology, 3 (3): 129-139 (1981).
5. Riggins, James. Investigation of High Power, Pulsed, Neodymium:YAG Lasers for Correcting Opacities of the Human Eye. MS Thesis. Wright-Patterson AFB, Ohio: Air Force Institute of Technology.
6. Lerman, Sidney. Preliminary Evaluation and Assessment of the Pulsed Nd:YAG Laser as a Non-Invasive Method to Disrupt Intraocular Membranes. Evaluation of Ocular Safety with Particular Respect to the Vitreous and Retina. Atlanta: Emory University School of Medicine, May 1982.
7. Hecht, E. and A. Zajac. Optics. Reading, Menlo Park, London, Amsterdam, Don Mills, and Sydney: Addison-Wesley Publishing Co., 1974.
8. Lerman, Sidney. Radiant Energy and the Eye. New York: MacMillan Publishing Co., Inc., 1980.
9. Gloor, B. P. "The Vitreous," Adler's Physiology of the Eye, edited by Robert A. Moses. Saint Louis: The C. V. Mosby Co., 1975.
10. Allen, R. G. "Retinal Thermal Injury," Ocular Effects of Non-Ionizing Radiation, Proceedings of the Society of Photo-Optical Instrumentation Engineers, 229: 80-86 (April 7, 1980).
11. Van der Zyper, E., et. al. "Changes in the Ultrastructure of the Iris After Irradiation with Intense Light," Advances in Ophthalmology, 39: 59-180 (1979).

12. Barnes, Frank S. "Applications of Lasers to Biology and Medicine," Proceedings of the IEEE, 63 (9): 1269-1277 (September 1975).
13. Sliney, David and Myron Wolbarsht. Safety with Lasers and Other Optical Sources. New York: Plenum Press, 1980.
14. Mendelson, Janice A. and Norman B. Ackerman. "Study of Biologically Significant Forces Following Laser Irradiation," Applied Physics Letters, 30 (2): 111-114 (15 January 1977).
15. Cleary, S. F. "Laser Pulses and the Generation of Acoustic Transients in Biological Material," Laser Applications in Medicine and Biology, Volume 3, edited by M. L. Wolbarsht, New York: Plenum Press, 1977.
16. Stamm, M. R. Physics of Laser Effects. Class Notes. PH 6.20. Spring Quarter, 1982. Wright-Patterson AFB, Ohio: Air Force Institute of Technology, March 1982.
17. Zel, dovich, Ya. B. and Yu. P. Raizer. Physics of Shock Waves and High-Temperature Hydrodynamic Phenomena. New York and London: Academic Press, 1966.
18. Harlow, F. H. and A. A. Amsden. Fluid Dynamics. LA-4700. Los Alamos, New Mexico: Los Alamos Scientific Laboratory, June 1971.
19. Shkarofsky, I. P. "Review of Gas-Breakdown Phenomena Induced by High-Power Lasers-I," RCA Review, 35: 48-77 (March 1974).
20. Barnes, Peter A. and K. E. Rieckhoff. "Laser Induced Underwater Sparks," Applied Physics Letter, 13 (8): 282-284 (October 15, 1968).
21. Bell, C. E. and J. A. Lanott. "Laser-Induced High-Pressure Shock Waves in Water," Applied Physics Letters, 10 (2): 46-48 (January 15, 1967).
22. Marshall, J. "Thermal and Mechanical Mechanisms in Laser Damage to the Retina," Investigative Ophthalmology, 9: 97-101 (1970).
23. Fraunfelder, F. T. and L. J. Viernstein. "Intraocular Pressure Variation During Xenon and Pulsed Ruby Laser Photocoagulation," American Journal of Ophthalmology, 71: 1261-1270 (1971).
24. Cleary, S. F. and P. E. Hamrick. "Laser-Induced Retinal Damage," Non-Ionizing Radiation, 2: 1-10 (1971).

25. Sedov, L. I. Similarity and Dimensional Methods in Mechanics. New York and London: Academic Press, 1959.
26. Brodie, R. N. and J. E. Hormuth. The PUFF 66 and P PUFF 66 Computer Programs. AFWL-TR-66-48. Kirtland AFB, New Mexico: Air Force Weapons Laboratory, May 1966.
27. Fisher, R. H. and H. E. Head. Rip, a One-Dimensional Material Response Code. DNA 2993F. La Jolla, California: Systems, Science, and Software, September 1972.
28. Richtmeyer, R. D. and K. W. Morton. Difference Methods for Initial-Value Problems (Second Edition). New York: Interscience Publishers, 1967.
29. Anderson, C. L. Jr. BEERAY, A One-Dimensional Hydrodynamics Code for Strong Shocks. MS Thesis. Wright-Patterson AFB, Ohio: Air Force Institute of Technology, December 1975.
30. YG470 Operating Manual. Santa Clara: Quantel International, 1982.
31. Reif, F. Fundamental of Statistical and Thermal Physics. New York, San Francisco, St. Louis, Toronto, London, and Sydney: McGraw-Hill Book Company, 1965.
32. Weast, R. C. and M. J. Astle, editors. CRC Handbook of Chemistry and Physics. Boca Raton: CRC Press, Inc., 1978.

APPENDIX A.

Calculation of γ for Water

One of the most important requirements in the initial stages of the development of EYESHOC was to obtain a value of γ -- the ratio of the specific heat at constant pressure to the specific heat at constant volume -- for water, as this was the basis of the model for the vitreous. This γ factor was required in the Grüneisen equation of state. The calculation is as follows, beginning with the relationship between C_p and C_v (Ref 31:168),

$$C_p - C_v = VT\alpha^2/\kappa \quad (A-1)$$

where

V is the volume (cm^3)

T is the absolute temperature ($^{\circ}\text{K}$)

α is the volume coefficient of expansion ($^{\circ}\text{K}^{-1}$)

κ is the isothermal compressibility (cm^3/erg)

For this calculation, these variables assumed the values (Ref 32:F-5),

$$V = 1 \text{ cm}^3$$

$$T = 310.15 \text{ }^{\circ}\text{K}$$

$$\alpha = 3.62 \times 10^{-4} / ^{\circ}\text{K}$$

$$\kappa = 4.45 \times 10^{-11} \text{ cm}^3/\text{erg}$$

Rearranging Equation (A-1), we obtain,

$$C_v = C_p - VT\alpha^2/\kappa \quad (A-2)$$

and for the absolute temperature given,

$$C_p = 4.1755 \times 10^7 \text{ erg/gm-}^\circ\text{C}$$

so that upon solution,

$$C_v = 4.0842 \times 10^7 \text{ erg/gm-}^\circ\text{C}$$

Finally, substituting these values of C_p and C_v into Equation (13), we obtain,

$$\gamma = 1.022$$

At this point, we should note that all of the calculations performed in this thesis are highly dependent upon the value of γ derived for water. If the equations are examined, it can be seen that the dependence of the Grüneisen equation of state appears as $(\gamma-1)$. For the value of γ obtained above, this is equal to 2.2×10^{-2} . If the value of γ is incorrect by as much as 0.01, the value of $(\gamma-1)$ is changed to 3.2×10^{-2} which is an increase of 45%, while the change in the value of γ is a mere 1%. Extreme care was taken in the calculation of γ as presented herein, however, it must be realized that even if a minor error is present in this calculation, it will be magnified by the equations in use.

APPENDIX B

Elimination of Specific Internal Energy in Time
Derivative of Pressure

Initially, the Grüneisen equation of state is expressed in terms of density rather than the specific volume V. Thus,

$$p = p_H + (\gamma - 1) \rho (E - E_H) \quad (B-1)$$

$$p_H = \rho_0 C^2 \rho (\rho - \rho_0) / [\rho - \frac{1}{2} \gamma (\rho - \rho_0)]^2 \quad (B-2)$$

$$E_H = \frac{1}{2} \left[C(\rho - \rho_0) / [\rho - \frac{1}{2} \gamma (\rho - \rho_0)] \right]^2 \quad (B-3)$$

Solving for E in the above equations,

$$E = [p / (\gamma - 1) \rho] - [p_H / (\gamma - 1) \rho] + E_H \quad (B-4)$$

$$E = \frac{p}{(\gamma - 1) \rho} + \left[\frac{C^2 [(\gamma - 1)(\rho - \rho_0)^2 - 2\rho_0(\rho - \rho_0)]}{2(\gamma - 1)[\rho(2 - \gamma) + (\gamma - 1)\rho_0]^2} \right] \quad (B-5)$$

Since the specific internal energy is a function only of pressure and density, the time derivative of the internal energy is then given by,

$$dE/dt = (\partial E / \partial p)(dp/dt) + (\partial E / \partial \rho)(d\rho/dt) \quad (B-6)$$

$$\partial E / \partial \rho = 1 / (\gamma - 1) \rho \quad (B-7)$$

$$\begin{aligned} \frac{\partial E}{\partial \rho} = \frac{p}{(\gamma - 1) \rho^2} + \frac{C^2}{(\gamma - 1)} & \left[\frac{[(\gamma - 1)(\rho - \rho_0) - \rho_0][\rho - (\gamma - 1)(\rho - \rho_0)]}{[\rho - (\gamma - 1)(\rho - \rho_0)]^3} \right. \\ & \left. + \frac{-[(\gamma - 1)(\rho - \rho_0)^2 - 2\rho_0(\rho - \rho_0)](2 - \gamma)}{[\rho - (\gamma - 1)(\rho - \rho_0)]^3} \right] \quad (B-8) \end{aligned}$$

Examining only the numerator of the terms in braces since they share a common denominator,

$$\begin{aligned} \text{numerator} = & [(\gamma-1)(\rho-\rho_0)\rho - \frac{1}{2}\gamma(\gamma-1)(\rho-\rho_0)^2 - \rho\rho_0 \\ & + (\gamma-1)\rho_0(\rho-\rho_0)] + [-(\gamma-1)(\rho-\rho_0)^2 + 2(\rho-\rho_0)\rho_0 \\ & + \frac{1}{2}\gamma(\gamma-1)(\rho-\rho_0)^2 - 2(\gamma-1)(\rho-\rho_0)\rho_0] \end{aligned} \quad (\text{B-9})$$

$$\text{numerator} = \rho_0 [(\gamma - \frac{1}{2}\gamma)(\rho - \rho_0) - \rho_0] \quad (\text{B-10})$$

$$\text{numerator} = \rho_0 [\frac{1}{2}\gamma(\rho - \rho_0) - \rho_0] \quad (\text{B-11})$$

Therefore, the time derivative of the specific internal energy is given by,

$$\frac{dE}{dt} = \frac{1}{(\gamma-1)} \frac{dp}{dt} + \left[-\frac{p}{(\gamma-1)\rho^2} + \frac{\rho_0 C^2}{(\gamma-1)} \frac{(\gamma-1)(\rho-\rho_0)\rho_0}{\rho - (\gamma-1)(\rho-\rho_0)} \right] \frac{d\rho}{dt} \quad (\text{B-12})$$

Solving for dp/dt ,

$$\frac{dp}{dt} = (\gamma-1)\rho \frac{dE}{dt} - \left\{ -\frac{p}{\rho} + \rho\rho_0 C^2 \left[\frac{\frac{1}{2}\gamma(\rho-\rho_0)\rho_0}{[\rho - \frac{1}{2}\gamma(\rho-\rho_0)]^3} \right] \right\} \frac{d\rho}{dt} \quad (\text{B-13})$$

or,

$$\frac{dp}{dt} = - \left\{ p + (\gamma-1)(p+q) - \rho^2 \rho_0 C^2 \left[\frac{\frac{1}{2}\gamma(\rho-\rho_0)\rho_0}{[\rho - \frac{1}{2}\gamma(\rho-\rho_0)]^3} \right] \right\} \nabla \cdot \mathbf{u} \quad (\text{B-14})$$

if the artificial viscosity and the value of $d\rho/dt$ are included.

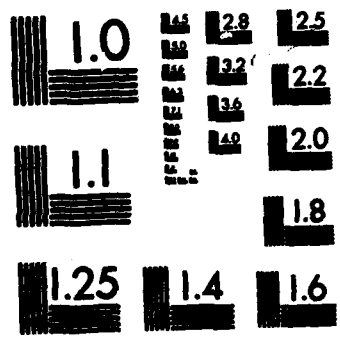
AD-A124 731

NEODYMIUM: YAG LASER INDUCED SHOCK WAVE OVERPRESSURES 2/2
AT THE RETINA(U) AIR FORCE INST OF TECH
WRIGHT-PATTERSON AFB OH SCHOOL OF ENGINEERING
J F TURNER DEC 82 AFIT/GEP/PH/82D-23 F/G 6/18 NL

UNCLASSIFIED



END
FORMED
BY
DTIC



MICROCOPY RESOLUTION TEST CHART
NATIONAL BUREAU OF STANDARDS-1963-A

APPENDIX C

Calculation of Time Step Based on Local Adiabatic Speed of Sound

The adiabatic speed of sound of a cell J at a time t can be written

$$C = (dp/d\rho)^{\frac{1}{2}} \quad (C-1)$$

which can be expressed as

$$C = [(dp/dt)/(d\rho/dt)]^{\frac{1}{2}} \quad (C-2)$$

Substituting Equations (1) and (B-14) into the above expression, we obtain,

$$C = \left\{ \frac{p + (\gamma-1)(p+q) - \frac{\rho^2 \rho_0 C [\frac{1}{2}\gamma(\rho-\rho_0)\rho_0]}{[\rho - \frac{1}{2}\gamma(\rho-\rho_0)]^3}}{\rho} \right\}^{\frac{1}{2}} \quad (C-3)$$

If we assume that C is constant over the time interval of interest, and if the shock wave is only allowed to cross one-fifth of a cell in a time unit Δt , then this Δt is given by,

$$\Delta t = 0.2(\Delta x) \left\{ \rho \left[p + (\gamma-1)(p+q) - \frac{\rho^2 \rho_0 C^2 [\frac{1}{2}\gamma(\rho-\rho_0)\rho_0]}{[\rho - \frac{1}{2}\gamma(\rho-\rho_0)]^3} \right]^{-1} \right\}^{\frac{1}{2}} \quad (C-4)$$

where,

Δx is the distance travelled by the boundary of the cell (cm).

It should be noted that if $\rho = \rho_0$, the value of the speed of sound reduces to

$$C = (\gamma p / \rho)^{\frac{1}{2}} \quad (C-5)$$

which is the ideal gas value of the speed of sound, without the artificial viscosity included, and the time Δt becomes

$$\Delta t = 0.2 (\Delta x) / (\gamma p / \rho)^{\frac{1}{2}}$$

APPENDIX D

Calculation of First Cell Specific Internal Energy and Pressure

For this example, consider an energy present in the laser pulse of 5 mJ:

$$E_0 = 5 \text{ mJ} = 5 \times 10^4 \text{ erg} \quad (\text{D-1})$$

If we consider a sphere of radius 100 microns, then the volume of this sphere is given by

$$V = \frac{4}{3} \pi r^3 \quad (\text{D-2})$$

or,

$$V = 4.189 \times 10^{-6} \text{ cm}^3$$

To determine the mass contained in this sphere, the volume is multiplied by the density ρ_0 , according to

$$m = \rho_0 V \quad (\text{D-3})$$

or,

$$m = 4.218 \times 10^{-6} \text{ gm}$$

To calculate the specific internal energy, we divide the pulse energy by the mass, so that

$$E = E_0 / m \quad (\text{D-4})$$

or,

$$E = 1.185 \times 10^{10} \text{ erg/g}$$

If we examine the Gruneisen equation of state, we see that at $t = t_0$, $\rho = \rho_0$, and therefore,

$$P_H = 0 \quad (D-5a)$$

$$E_H = 0 \quad (D-5b)$$

and

$$p = \rho_0(\gamma - 1)E \quad (D-6)$$

or,

$$p = 2.625 \times 10^8 \text{ erg/cm}^3$$

APPENDIX E

EYESHOC Code Listing and Sample Output

This appendix provides the complete code listing for EYESHOC, along with a complete list of the variables used in the code. In addition, the output generated by the program is illustrated in Figure E-1.

THIS CODE MODELS THE ONE-DIMENSIONAL PROPAGATION OF A SHOCK WAVE IN THE HUMAN EYE. THE SHOCK IS CAUSED BY FOCUSING A ND:YAG LASER IN OR NEAR THE POSTERIOR CAPSULE OF THE EYE TO REMOVE OPACITIES IN THE CAPSULE. THIS CODE USES A LAGRANGIAN MESH TO DESCRIBE THE PROPAGATION. THE SHOCK IS ALLOWED TO PROPAGATE TO THE RETINA, WITH EMPHASIS BEING PLACED ON THE AMPLITUDE OF THE PRESSURE FRONT AT THE RETINA IN AN EFFORT TO QUANTITATIVELY ESTIMATE THE MAXIMUM LASER FLUX WHICH CAN SAFELY BE DEPOSITED IN THE POSTERIOR CAPSULE AND NOT CAUSE RETINAL DETACHMENT.

PROGRAM EYESHOC (INPUT, OUTPUT, TAPE6=OUTPUT)

DEFINITION OF VARIABLES

A - FACTOR EQUAL TO APPROXIMATELY ONE-HALF THE NUMBER OF CELLS OVER WHICH THE SHOCK IS TO BE SPREAD
ALPHA - FACTOR WHICH DETERMINES THE CODE GEOMETRY, WHERE
ALPHA = 1 FOR CARTESIAN COORDINATES
ALPHA = 2 FOR CYLINDRICAL COORDINATES
ALPHA = 3 FOR SPHERICAL COORDINATES
DELT - TIME STEP FOR EACH CYCLE
DT - INDIVIDUAL TIME STEP VALUES, THE MINIMUM OF WHICH IS DELT
DX - WIDTH OF EACH CELL (CM)
E - INTERNAL ENERGY (ERG/GM)
EM - INTERNAL ENERGY CORRECTION FACTOR DEPENDENT ON CHANGE IN DENSITY DUE TO SHOCK WAVE
F - COMPRESSION FACTOR INCLUDED TO CONSIDER BOUNDARY SHIFTS
FPM - STORAGE FILE FOR F VALUE OF EACH PASS
FRAC1 - EXPERIMENTALLY DETERMINED CONSTANT RANGING FROM 0.1 TO 0.5
GAMMA - RATIO OF SPECIFIC HEATS (CP/CV)
GAMP-M - GAMMA MINUS ONE
J - CELL NUMBER
OLDV - VELOCITY VALUES DETERMINED ON PREVIOUS PASS (CM/SEC)
OLDX - POSITION VALUES DETERMINED ON PREVIOUS PASS (CM)
P - PRESSURE IN CELL J (ERG/CM**3)
PH - PRESSURE CORRECTION FACTOR DEPENDENT ON CHANGE IN DENSITY DUE TO SHOCK WAVE
Q - ARTIFICIAL VISCOSITY FACTOR USED TO DEFINE A CLEAN SHOCK FRONT
RHO - DENSITY OF CELL J (GM/CM**3)
T - TEMPERATURE OF CELL J (DEG K)
TIME - TOTAL ELAPSED TIME SINCE LASER ENERGY DEPOSITION (SEC)
UDOT - ACCELERATION OF CELL J (CM/SEC**2)
V - VELOCITY OF BOUNDARY OF CELL J (CM/SEC)
X - BOUNDARY OF CELL J (CM)

DIMENSION X(50), P(50), Q(50), V(50), R(50), DT(50), T(50), E(50)
DIMENSION UDOT(50), OLDX(50), OLDV(50), EM(50), PH(50), DX(50)
DIMENSION ALUM(50), SPEED(50)
INTEGER CYCLE

INITIALIZATION OF VARIABLES

A = 1.

```

ALPHA = 3.
FRAC = 0.2
GAMP M = 2.2E-2
TIME = 0.
DX(1) = 1.0E-2
DO 5 J = 2, 50
5   DX(J) = 1.10*DX(J-1)
   X(1) = 0.
   DO 10 J = 2, 45
     DT(J-1) = 0.
     E(J-1) = 4.69E7
     P(J-1) = 1.04E6
     Q(J-1) = 0.
     RO(J-1) = 1.007
     T(J-1) = 310.15
     V(J-1) = 0.
     X(J) = X(J-1)+DX(J-1)
10  CONTINUE
   E(1) = 5.33E10
   P(1) = 1.18E9
   PRINT 900
   WRITE (6,910) (J, X(J), V(J), P(J), RO(J), Q(J), T(J), D*(J),
   *E(J), J = 1, 40)

```

```

CYCLE = 1.
DO 100 CYCLE = 1, 2000

```

CALCULATION OF TIME STEP

```

DELT = 500.
DO 20 J = 1, 40
  ANUM(J) = P(J)+(P(J)+Q(J))*GAMP M-(RO(J)**2*2.34E10*(0.511*
  *(RO(J)-1.007)-1.007)/(RO(J)-0.511*(RO(J)-1.007))**3)
  SPEED(J) = SQRT(ANUM(J)/RO(J))
  DT(J) = FRAC*(X(J+1)-X(J))/SPEED(J)
20  IF (DT(J) .LT. DELT) DELT = DT(J)

```

CALCULATION OF CELL BOUNDARY ACCELERATION AND NEW VELOCITY VALUES WHILE RETAINING OLD POSITION AND VELOCITY VALUES

```

UDOT(1) = 0.
DO 30 J = 1, 40
30  UDOT(J+1) = -4*(P(J+1)+Q(J+1)-P(J)-Q(J))/((X(J+2)-X(J))*
  *(RO(J+1)+RO(J)))
DO 40 J = 1, 45
40  OLDV(J) = V(J)
   OLDX(J) = X(J)
DO 50 J = 1, 40
50  V(J+1) = V(J+1)+UDOT(J+1)*DELT

```

CALCULATION OF NEW CELL BOUNDARIES, COMPRESSION FACTOR F, DENSITY, ARTIFICIAL VISCOSITY, AND PRESSURE VALUES

```

DO 60 J = 1, 40
  X(J+1) = X(J+1)+((OLDV(J+1)+V(J+1))/2)*DELT
  F = ((OLDX(J+1)**ALPHA-(OLDX(J)**ALPHA))/((X(J+1)**ALPHA
  *(X(J)**ALPHA)))

```

```

      FPM = F
      IF (FPM .LE. 1.) FPM = 1.
      RJ(J) = R0(J)*F
      Q(J) = A**2*R0(J)*((X(J+1)-X(J))**2)*(DELT**(-2))
      **((1.-FPM)**2)
50     P(J) = P(J)-ANUM(J)*(1.-F)

```

CALCULATION OF NEW ENERGY AND TEMPERATURE VALUES

```

      DO 70 J = 1, 40
      PH(J) = (2.30E10-2.32E10/R0(J))*(0.4856+0.511/R0(J))**(-2)
      EH(J) = 0.5*((1.51E5-1.52E5/R0(J))/(0.4856+0.511/R0(J)))**2
      E(J) = ((P(J)-PH(J))/0.511*R0(J))+EH(J)
70     T(J) = T(J) + E(J)/1.593E6
      TIME = TIME+DELT

```

PRINT ROUTINE FOR RESULTS

```

      IF (MOD(CYCLE, 10) .NE. 0.) GO TO 100
      WRITE (6,500) CYCLE, TIME
00     FORMAT (1X, 'PUN = ', T7, I4, 4X, 'TIME = ', 1PE9.3)
      PRINT 900
00     FORMAT (T10, 'X', T20, 'V', T30, 'P', T40, 'R0', T50, 'Q', T60
      'T', T70, 'DT', T80, 'E')
      WRITE(6,910) (J, X(J), V(J), P(J), R0(J), Q(J), T(J), DT(J),
      'E(J), J = 1, 40)
10     FORMAT (1X, I3, 1PE10.2)
100    CONTINUE
      STOP
      END

```

RUN = 250 TIME = 3.274E-06

K	M	V	P	RG	Q	T	DT	E
1	0.	0.	-7.28E+03	9.53E-01	1.77E+03	3.37E+03	1.35E-04	1.07E+09
2	1.02E-02	-1.43E+04	7.35E+06	1.01E+00	2.97E+03	4.36E+02	1.42E-08	5.61E+07
3	2.13E-02	-1.35E+04	-1.44E+05	1.00E+00	0.	4.40E+02	1.55E-08	7.17E+07
4	3.32E-02	6.06E+03	-2.06E+04	9.58E-01	4.17E+07	4.36E+02	1.77E-08	7.59E+07
5	4.65E-02	-1.19E+03	3.02E+05	1.02E+00	8.74E+05	4.35E+02	1.90E-08	8.39E+07
6	6.13E-02	-1.05E+03	-1.94E+08	9.99E-01	0.	4.35E+02	2.13E-08	7.81E+07
7	7.72E-02	5.95E+02	5.51E+07	1.01E+00	3.50E+05	4.35E+02	2.32E-08	6.01E+07
8	9.49E-02	-4.26E+01	-1.63E+07	1.01E+00	1.59E+03	4.35E+02	2.56E-08	7.93E+07
9	1.14E-01	-9.13E+01	1.00E+07	1.01E+00	0.	4.35E+02	2.81E-08	7.95E+07
10	1.35E-01	2.20E+01	-1.79E+06	1.01E+00	0.	4.35E+02	3.09E-08	7.94E+07
11	1.59E-01	6.55E+01	5.91E+06	1.01E+00	6.17E+03	4.35E+02	3.40E-08	7.95E+07
12	1.85E-01	-1.55E+01	2.74E+06	1.01E+00	0.	4.35E+02	3.74E-08	7.95E+07
13	2.14E-01	-3.89E+00	-5.33E+06	1.01E+00	0.	4.35E+02	4.12E-08	7.94E+07
14	2.43E-01	-4.49E+00	3.42E+06	1.01E+00	0.	4.35E+02	4.53E-08	7.95E+07
15	2.70E-01	3.47E+00	-1.20E+05	1.01E+00	9.87E+00	4.35E+02	4.98E-08	7.94E+07
16	3.12E-01	-9.59E-01	1.83E+06	1.01E+00	0.	4.35E+02	5.48E-08	7.95E+07
17	3.59E-01	2.49E+00	6.99E+05	1.01E+00	2.87E+01	4.35E+02	6.03E-08	7.94E+07
18	4.05E-01	-2.97E+00	6.64E+05	1.01E+00	0.	4.35E+02	6.63E-08	7.94E+07
19	4.55E-01	8.20E-01	1.21E+06	1.01E+00	0.	4.35E+02	7.29E-08	7.94E+07
20	5.12E-01	9.23E-01	1.11E+06	1.01E+00	0.	4.35E+02	8.02E-08	7.94E+07
21	5.73E-01	2.03E-01	1.05E+06	1.01E+00	3.50E-01	4.35E+02	8.83E-08	7.94E+07
22	6.40E-01	2.10E-02	1.04E+06	1.01E+00	2.37E-02	4.35E+02	9.71E-08	7.94E+07
23	7.14E-01	1.22E-03	1.04E+06	1.01E+00	-2.80E-04	4.35E+02	1.07E-07	7.94E+07
24	7.95E-01	4.41E-05	1.04E+06	1.01E+00	9.34E-07	4.35E+02	1.17E-07	7.94E+07
25	8.85E-01	1.03E-05	1.04E+06	1.01E+00	1.29E-03	4.35E+02	1.29E-07	7.94E+07
26	9.83E-01	9.02E-09	1.04E+06	1.01E+00	9.71E-13	4.35E+02	1.42E-07	7.94E+07
27	1.04E+00	0.	1.04E+06	1.01E+00	0.	4.35E+02	1.56E-07	7.94E+07
28	1.21E+00	0.	1.04E+05	1.01E+00	0.	4.35E+02	1.72E-07	7.94E+07
29	1.34E+00	0.	1.04E+05	1.01E+00	0.	4.35E+02	1.89E-07	7.94E+07
30	1.49E+00	0.	1.04E+06	1.01E+00	0.	4.35E+02	2.08E-07	7.94E+07
31	1.64E+00	0.	1.04E+06	1.01E+00	0.	4.35E+02	2.29E-07	7.94E+07
32	1.82E+00	0.	1.04E+05	1.01E+00	0.	4.35E+02	2.52E-07	7.94E+07
33	2.01E+00	0.	1.04E+05	1.01E+00	0.	4.35E+02	2.77E-07	7.94E+07
34	2.22E+00	0.	1.04E+05	1.01E+00	0.	4.35E+02	3.05E-07	7.94E+07
35	2.45E+00	0.	1.04E+05	1.01E+00	0.	4.35E+02	3.35E-07	7.94E+07

Figure E-1. Sample Output from EYESHOC

APPENDIX F

Modeling a Point Explosion Using EYESHOC

In order to determine the validity of the code EYESHOC, a point explosion was modeled using the code and was compared to the results obtained by Sedov (Ref 25:238-248).

Sedov defines his shock relations in terms of ratios of pressure, density, radius, or velocity parameters, such that the comparison of all shock relations can be made using these dimensionless variables. In the validation of EYESHOC, the ratios used were p_2/p_1 , ρ_2/ρ_1 , and r_2/r^0 . These are defined according to

p_2 is the maximum pressure of the shock

p_1 is the ambient pressure of the medium

ρ_2 is the maximum density of the shock

ρ_1 is the ambient density of the medium

r_2 is the radial distance to the point of maximum pressure of the shock

and

$$r^0 = (E_0/p_1)^{1/3} \quad (F-1)$$

where

E_0 is the energy of the pulse in ergs

To validate EYESHOC based on the dimensionless variables introduced herein, a point explosion was modeled for an ideal

gas with $\gamma = 1.4$. This was used rather than the Grüneisen equation of state and $\gamma = 1.022$ so that the results of the comparison would be apparent and not hidden because of the differences in the conditions of the test. Figures F-1 and F-2 present the results of this comparison. The comparison was made for an energy $E_0 = 7.19 \times 10^{20}$ erg and a value of $r^0 = 1.1 \times 10^5$ cm. As is noted in both cases, examination of the pressure drop across the front and the density behind the front as a function of shock wave radius, the dashed line and all points plotted are EYESHOC results, while Sedov predictions are indicated by the solid line. For much of the range covered in both cases, it is virtually impossible to distinguish between the two lines, indicating excellent agreement between EYESHOC results and the theory presented by Sedov.

Based on this comparison, it is obvious that EYESHOC is valid in its treatment of a point explosion. If the assumptions of Chapter IV are valid, then the code can be assumed to be usable for its intended purpose.

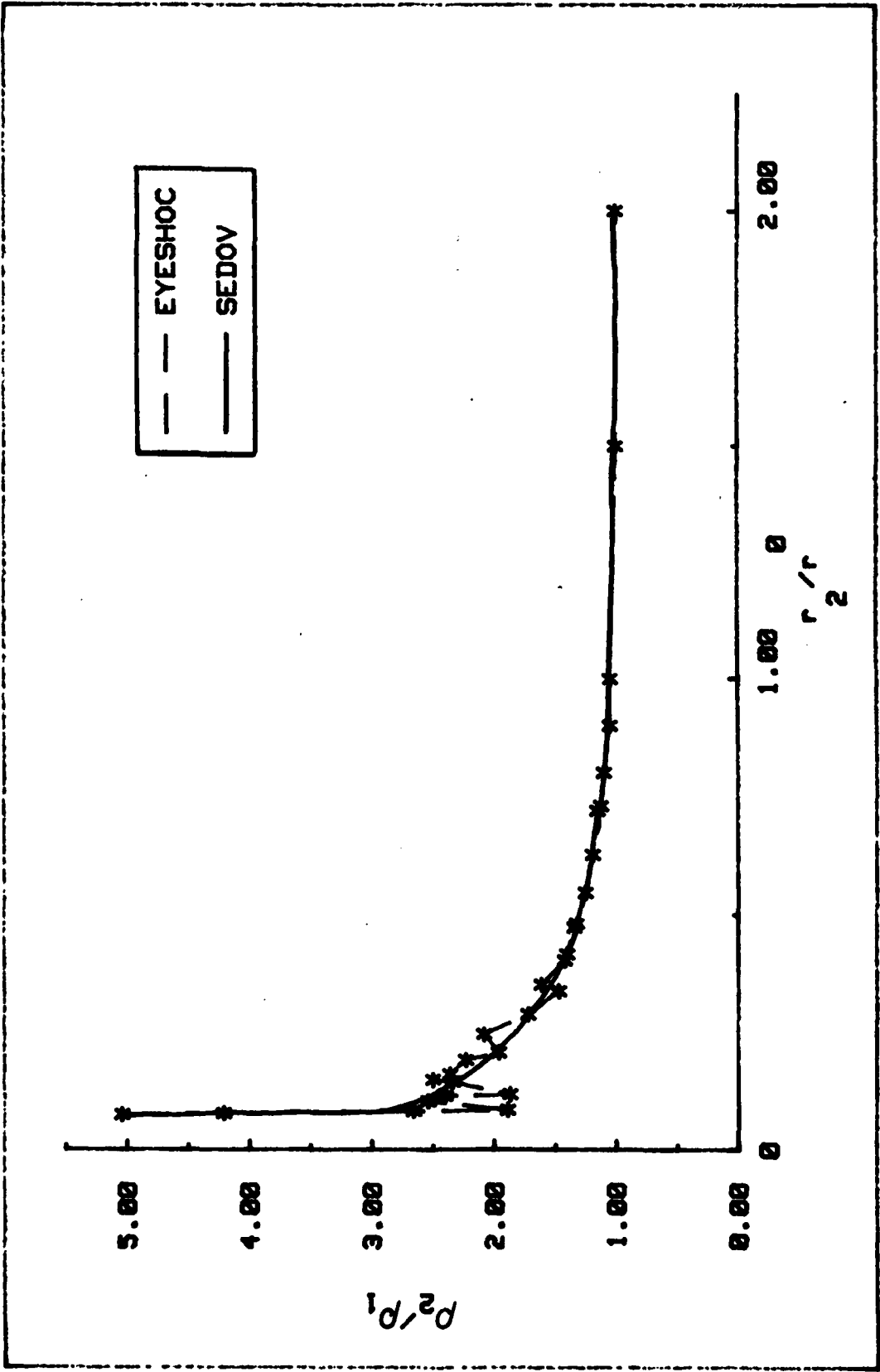


Figure F-1. Comparison of Pressure Drop Across Front versus Shock Wave Radius for EYESHOC and Sedov

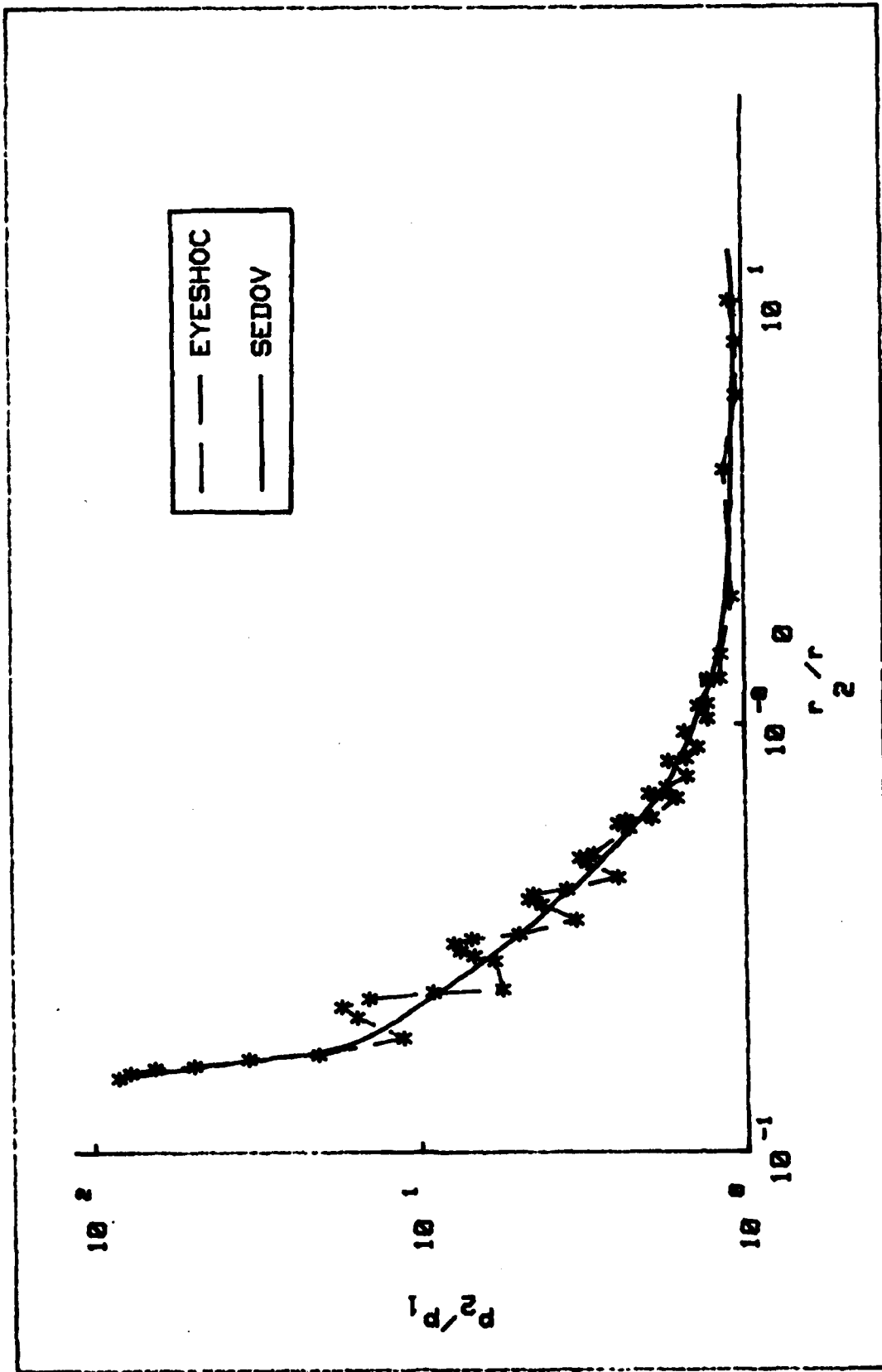


Figure F-2. Comparison of Density Behind Wave Front versus Shock Wave Radius for EYESHOC and Sedov

Vita

John Franklin Turner was born 4 September 1960 in Atlanta, Georgia. He graduated from North Clayton Senior High School in 1978 after having completed his freshmen year at the Georgia Institute of Technology. In June 1981, he graduated with honors, receiving Bachelor of Science degrees in Applied Physics and Applied Biology, as well as a commission as a Second Lieutenant in the Air Force through the ROTC program. Later that month, he entered the School of Engineering, Air Force Institute of Technology, to pursue a Master of Science degree in Engineering Physics.

Permanent Address: 3002 D Bedevere Circle
Decatur, Georgia 30035

UNCLASSIFIED

SECURITY CLASSIFICATION OF THIS PAGE (When Data Entered)

REPORT DOCUMENTATION PAGE		READ INSTRUCTIONS BEFORE COMPLETING FORM
1. REPORT NUMBER AFIT/GEP/PH/82D-23	2. GOVT ACCESSION NO. A124 73	3. RECIPIENT'S CATALOG NUMBER
4. TITLE (and Subtitle) NEODYMIUM:YAG LASER INDUCED SHOCK WAVE OVERPRESSURES AT THE RETINA		5. TYPE OF REPORT & PERIOD COVERED MS THESIS
		6. PERFORMING ORG. REPORT NUMBER
7. AUTHOR(s) JOHN F. TURNER 2LT USAF		8. CONTRACT OR GRANT NUMBER(s)
9. PERFORMING ORGANIZATION NAME AND ADDRESS AIR FORCE INSTITUTE OF TECHNOLOGY (AFIT/EN) WRIGHT-PATTERSON AFB, OHIO 45433		10. PROGRAM ELEMENT, PROJECT, TASK AREA & WORK UNIT NUMBERS
11. CONTROLLING OFFICE NAME AND ADDRESS		12. REPORT DATE DECEMBER 1982
		13. NUMBER OF PAGES 110
14. MONITORING AGENCY NAME & ADDRESS (if different from Controlling Office)		15. SECURITY CLASS. (of this report) UNCLASSIFIED
		15a. DECLASSIFICATION/DOWNGRADING SCHEDULE
16. DISTRIBUTION STATEMENT (of this Report) APPROVED FOR PUBLIC RELEASE; DISTRIBUTION UNLIMITED		
17. DISTRIBUTION STATEMENT (of the abstract entered in Block 20, if different from Report)		
18. SUPPLEMENTARY NOTES Approved for public release; LAW AFR 190-17. <i>Lynn E. Wolaver</i> LYNN E. WOLAVER Dean for Research and Professional Development Air Force Institute of Technology (ATC) Wright-Patterson AFB OH 45433 19 JAN 1983		
19. KEY WORDS (Continue on reverse side if necessary and identify by block number) NEODYMIUM:YAG LASER RETINA SHOCK WAVE		
20. ABSTRACT (Continue on reverse side if necessary and identify by block number) The use of a neodymium:YAG laser to open opacified posterior capsules in the human eye was examined. In particular, this study involved the development of a one-dimensional hydrodynamic code to model the propagation of the shock wave in the vitreous, and the measurement of overpressures induced in a model system. The model system consisted of balanced salt solution in a cubical test cell. A pressure transducer was affixed to the rear of the		

DD FORM 1 JAN 73 1473 EDITION OF 1 NOV 65 IS OBSOLETE

UNCLASSIFIED

SECURITY CLASSIFICATION OF THIS PAGE (When Data Entered)

UNCLASSIFIED

SECURITY CLASSIFICATION OF THIS PAGE(When Data Entered)

cell, and 15 nsec Q-switched laser pulses were focused at distances of 6, 8, 10, and 14 mm from the transducer to initiate shock waves. Overpressures were measured for pulse energies of 3.75, 7.50, and 22.50 mJ at the focal point. The balanced salt solution was chosen because it resembles the vitreous in breakdown characteristics, and the 14 mm distance is significant since it approximates the distance from the posterior capsule to the retina.

Overpressures ranging from 0.018 - 0.432 atm were recorded at the transducer. The code was tested for a pulse energy of 3.75 mJ and predicted a pressure change of 2%, in excellent agreement with measured values. For pulse energies of 7.50 and 22.50 mJ, the maximum deviation was 5% from measured pressure differences.

Based on current research by ophthalmologists using such laser systems for treatment, it is concluded that overpressures of 0.10 atm or less cause no retinal damage.

UNCLASSIFIED

SECURITY CLASSIFICATION OF THIS PAGE(When Data Entered)